Mon. Not. R. Astron. Soc. **399,** 323–339 (2009) doi:10.1111/j.1365-2966.2009.15273.x

The UV-Excess survey of the northern Galactic plane

Paul J. Groot,[1⋆] Kars Verbeek,[1] Robert Greimel,[2,3] Mike Irwin,[4] Eduardo González-Solares,[4] Boris T. Gänsicke,[5] Eelco de Groot,[1] Janet Drew,[6] Thomas Augusteijn,[7] Amornrat Aungwerojwit,[5,8] Mike Barlow,[9] Susana Barros,[5] Else J. M. van den Besselaar,[1] Jorge Casares,[10] Romano Corradi,[2,10] Jesús M. Corral-Santana,[10] Niall Deacon,[1] Wilbert van Ham,[1] Haili Hu,[1] Uli Heber,[11] Peter G. Jonker,[12,13] Rob King,[14] Christian Knigge,[15] Antonio Mampaso,[10] Tom R. Marsh,[5] Luisa Morales-Rueda,[1] Ralf Napiwotzki,[6] Tim Naylor,[14] Gijs Nelemans,[1] Tim Oosting,[1] Stylianos Pyrzas,[2,5] Magaretha Pretorius,[16] Pablo Rodríguez-Gil,[2,10] Gijs H. A. Roelofs,[13] Stuart Sale,[17] Pim Schellart,[1] Danny Steeghs,[5,13] Cezary Szyszka,[18] Yvonne Unruh,[17] Nicholas A. Walton,[4] Simon Weston,[6] Andrew Witham,[15] Patrick Woudt[19] and Albert Zijlstra[20]

[1]*Department of Astrophysics, IMAPP, Radboud University Nijmegen, PO Box 9010, 6500 GL Nijmegen, the Netherlands*
[2]*Isaac Newton Group of Telescopes, Apartado de Correos 321, E-38700 Santa Cruz de La Palma, Canary Islands, Spain*
[3]*Institut für Physik, Karl-Franzen Universität Graz, Universitätsplatz 5, 8010 Graz, Austria*
[4]*Cambridge Astronomy Survey Unit, Institute of Astronomy, University of Cambridge, Madingley Road, Cambridge CB3 0HA*
[5]*Physics Department, University of Warwick, Coventry CV4 7AL*
[6]*Centre for Astronomy Research, Science and Technology Research Institute, University of Hertfordshire, Hatfield AL10 9AB*
[7]*Nordic Optical Telescope, Apartado 474, E-38700 Santa Cruz de La Palma, Canary Islands, Spain*
[8]*Department of Physics, Faculty of Science, Naresuan University, Phitsanulok 65000, Thailand*
[9]*Department of Physics and Astronomy, University College London, Gower Street, London WC1E 6BT*
[10]*Instituto de Astrofísica de Canarias, C/ Via Lactea, s/n, E38205 La Laguna, Tenerife, Spain*
[11]*Dr. Remeis-Sternwarte Bamberg, Universität Erlangen-Nürnberg, Sternwartstrasse 7, D-96049 Bamberg, Germany*
[12]*SRON, Netherlands Institute for Space Research, Sorbonnelaan 2, 3584 CA Utrecht, the Netherlands*
[13]*Harvard–Smithsonian Center for Astrophysics, 60 Garden Street, Cambridge, MA 02138, USA*
[14]*School of Physics, University of Exeter, Exeter EX4 4QL*
[15]*School of Physics and Astronomy, University of Southampton, Southampton, Hampshire SO17 1BJ*
[16]*South African Astronomical Observatory, Observatory, Cape Town, South Africa*
[17]*Imperial College of Science, Technology and Medicine, Blackett Laboratory, London SW7 2AZ*
[18]*European Southern Observatory, Karl-Schwarzschild-Strasse 2, D-85748 Garching bei München, Germany*
[19]*Department of Astronomy, University of Cape Town, Private Bag, Rondebosch 7700, Republic of South Africa*
[20]*Jodrell Bank Center for Astrophysics, School of Physics and Astronomy, University of Manchester, Manchester M13 9PL*

Accepted 2009 June 18. Received 2009 June 17; in original form 2009 May 18

ABSTRACT

The UV-Excess survey of the northern Galactic plane images a $10^\circ \times 185^\circ$ wide band, centred on the Galactic equator using the 2.5-m Isaac Newton Telescope in four bands (U, g, r, He I 5875) down to ∼21–22 mag (∼20 in He I 5875). The setup and data reduction procedures are described. Simulations of the colours of main-sequence stars, giant, supergiants, DA and DB white dwarfs and AM Canum Venaticorum stars are made, including the effects of reddening. A first look at the data of the survey (currently 30 per cent complete) is given.

Key words: surveys – stars: general – ISM: general – Galaxy: disc – Galaxy: stellar content – Galaxy: structure.

1 INTRODUCTION

The availability of wide-field CCD camera arrays on medium-sized telescopes has led to the emergence of large-scale optical surveys of

⋆E-mail: pgroot@astro.ru.nl

the sky, targeting one or more scientific objectives. The vast majority of these surveys, such as the Sloan Digital Sky Survey (SDSS; York et al. 2000), are concentrated on the extragalactic Universe. However, there is an increasing interest in a more detailed study of our own Milky Way Galaxy as well. The recently completed SDSS II/SEGUE programme (Yanny et al. 2009) is specifically targeting lower Galactic latitudes, and the RAVE survey (Steinmetz et al. 2006) is targeting the Galactic halo and streams and companions to the Milky Way.

The plane of the Milky Way, however, has so far not been the target of a full-scale optical, multicolour, digital and photon-noise-limited survey, despite its obvious value for many fields of astrophysics. This situation is changing with the European Galactic Plane Surveys (EGAPS) currently underway. Combined, the EGAPS (described below) will cover the full Galactic plane in a strip of $10^\circ \times 360^\circ$ centred on the Galactic equator, in the u/U, g, r, i, Hα bands down to (Vega) magnitude $\sim$21–22 (or equivalent line flux), and for the northern survey also in the He I 5875 filter. The EGAPS started off with the INT Photometric Hα Survey (IPHAS; Drew et al. 2005, hereafter D05) that covers the northern Galactic plane in the r, i and Hα bands. Here, we describe the UVEX survey: the UV-Excess survey of the northern Galactic plane that uses the exact same setup as the IPHAS but will image the northern plane in U, g, r and He I 5875. The southern Galactic plane will be covered by the VPHAS+ survey (using u, g, r, i, Hα) as an European Southern Observatory (ESO) Public Survey on the VST+Omegacam combination and will probably start in the beginning of 2010.

Very few dedicated blue surveys at low Galactic latitudes exist, apart from all-sky surveys, such as the Palomar sky surveys or the ESO sky surveys, performed in the 1950–1990s, using photographic plates. A notable exception is the Sandage two-colour survey of the Galactic plane as presented in a series of papers by Lanning (1973) and Lanning & Meakes (2004 and references therein; also see Lanning & Lépine 2006). The total survey covers 5332 deg^2 (124 plates) centred on the Galactic plane (at $b = -6^\circ$, 0° and $+6^\circ$) using photographic plates (6.°6 on a side) and the UG1 (UV) and GG13 (B) filters on the Palomar 48-inch Oschin Schmidt Telescope. So far 734 bright sources in 39 per cent of the total area of the survey have been published, averaging one source per 2.83 deg^2 down to $m_B \sim 20$. Ultraviolet (UV)-bright candidates were selected by eye as having $U - B < 0$, but with significant scatter on both the photometry and the completeness due to crowding and differing quality of the photographic plates. Not being digital combined with the extra problems crowding present to photographic observations, makes the survey good for picking out the bluest objects, but not useful for a systematic study of stellar populations in the Galactic plane. Although UVEX will cover a smaller area (1850 deg^2 for the northern survey; 3600 deg^2 when ultimately combined with the VPHAS+), the survey is fully photometric, allowing a more consistent and more detailed source extraction and all data will be digitally available. First results on the selection of UV-bright sources in UVEX show a much higher surface density of sources ($\sim$10 deg^{-2}), which is due to both the greater depth of UVEX (in particular in the g band) and the more consistent and automated selection techniques, which allow identification of UV-bright objects at a much redder cut-off than was possible for the Sandage two-colour survey (see Groot et al., in preparation).

Here, we describe the scientific objectives of the UVEX survey (Section 2), the survey design and observing strategy (Section 3), simulations of stellar populations in the UVEX colours (Section 4), the early results (Section 5), the seeing statistics and the effect of crowding on the detected number counts (Section 6) and conclusions (Section 7).

2 SCIENCE GOALS

The main science goal of UVEX is to chart the Galactic population of stellar remnants, single and in binary systems. These include single and binary white dwarfs, subdwarf B stars, cataclysmic variables, AM Canum Venaticorum (AM CVn) stars and neutron star and black hole binaries. These systems are hot, and therefore blue, due to the remnant energy in the compact objects or they are being kept hot due to accretion. Due to their small size (typically $\lesssim$1 R$_\odot$), these systems are intrinsically faint, despite their hot temperature. In particular, they have much lower absolute visual magnitudes than main-sequence stars of similar colours. At a given apparent magnitude, they will therefore be much closer by than main-sequence stars and therefore have suffered much less extinction than a main-sequence star of the same intrinsic colour. This technique to identify stellar remnants has been used before, for example, to search for old halo white dwarfs in front of molecular clouds (Hodgkin et al., private communication). The reason to survey the Galactic plane is that the target populations are Galactic populations, and therefore strongly concentrated towards the Galactic plane. Fig. 1 illustrates this point. Here, we have taken a model of the Galaxy according to the prescription of Boissier & Prantzos (1999), and populated this with populations having absolute visual magnitudes of $M_V =$ 15, 10 and 5. A Sandage (1972) type model of Galactic extinction was included. This Galaxy model is identical to the one used and described more extensively in Nelemans, Yungelson & Portegies Zwart (2004). A limiting magnitude of $V = 23$ was taken to construct Fig. 1. It can be seen that any population with an absolute magnitude in the range $5 \leq M_V \leq 10$ is strongly concentrated to the plane of the Galaxy. Respectively, 12, 40 and 97 per cent of all objects in Fig. 1 lie within the first 5° of the plane (the limits of the UVEX survey) for $M_V = 15$, 10 and 5. Subdwarf B stars, cataclysmic variables, AM CVn stars, young white dwarfs and most neutron star and black hole binaries all have absolute magnitudes $M_V < 15$. It is only for the faintest systems (old white dwarfs and very low mass accretion rate interacting binaries) that we sample such a local population that no concentration towards the Galactic plane is seen.

The prime motivation to chart the population of interacting binaries and stellar remnants in our Galaxy is that a large and homogeneous sample is needed to answer questions in the fields of binary stellar evolution (e.g. on the physics of the common-envelope phase), the gravitational radiation foreground from compact binaries in our Galaxy for missions such as the Laser Interferometer Space Antenna (LISA), and the influence of chemical composition on the accretion disc physics. For this last item in particular, the comparison between hydrogen-rich systems such as cataclysmic variables and helium-rich (AM CVn stars; e.g. Roelofs et al. 2006a) or even C/O-rich (ultracompact X-ray binaries; Nelemans et al. 2004a) systems will be important. The currently known populations of these last two classes are limited to less than two dozen systems each, severely limiting a population study (see Roelofs, Nelemans & Groot 2007).

Besides the main science goal outlined above, the UVEX survey will allow for many more scientific studies in the field of Galactic astrophysics, especially in combination with the IPHAS. The combination of UVEX and IPHAS will allow a much cleaner separation of stellar populations with different intrinsic colours, absolute

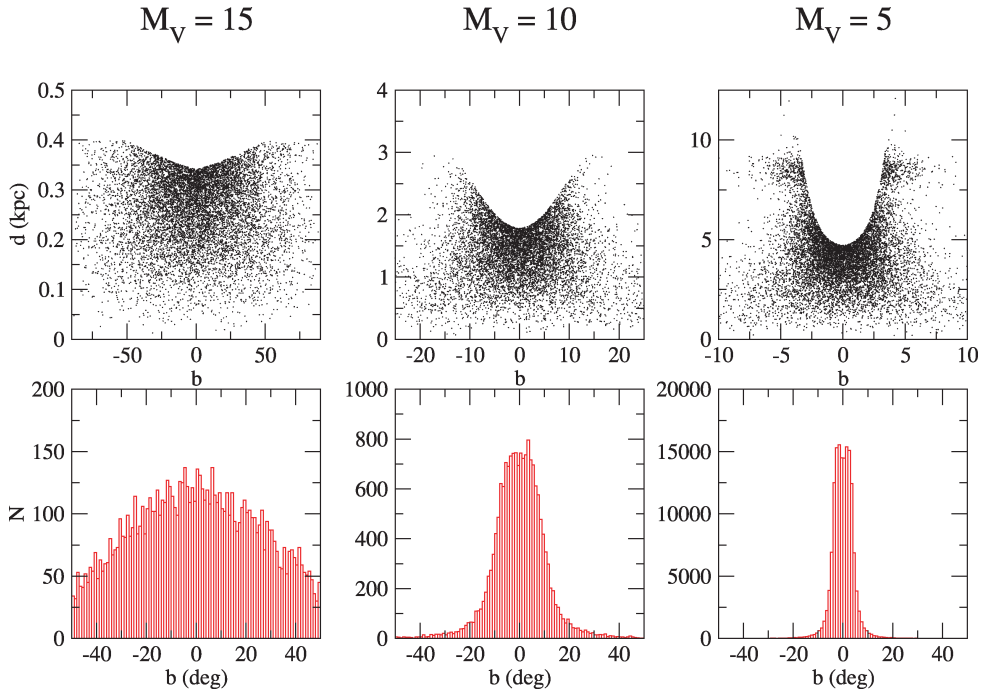

Figure 1. Distribution as a function of heliocentric distance versus latitude (upper panels) and a histogram of number of systems versus latitude (lower panels) of three Galactic populations with absolute visual magnitudes $M_V = 15$, 10 and 5 (left- to right-hand panels), based on a Galaxy model according to Boissier & Prantzos (1999), and including a Sandage (1972) extinction model, as detailed in Nelemans et al. (2004). A sample with limiting magnitude $V = 23$ is shown here to illustrate the strong concentration of these populations towards the Galactic plane. In the $M_V = 5$ panel, the extra sources at $d = 8$ kpc are caused by the Galactic bulge.

magnitudes and varying degrees of reddening. The added opportunities include the following.

(i) A three-dimensional dust model of our Galaxy on an arcsecond scale: the inclusion of Hα with the four broad-bands allows for breaking the degeneracy between reddened early-type stars and unreddened late-type stars due to their strongly different Hα absorption lines strength. See Drew et al. (2008) and Sale et al. (2009) for the usage of IPHAS data towards this goal.

(ii) The first-ever accurate high proper motion study in the Galactic plane. The overlap in *r*-band observations between UVEX and IPHAS has a minimum of 3-year baseline distance, and otherwise identical setup allows for proper motion determinations down to $\mu \geq 100$ mas yr^{-1} for the IPHAS–UVEX comparison and down to $\mu \geq 20$ mas yr^{-1} for an IPHAS–POSS I comparison (Deacon et al. 2009). These should be compared to the recent surveys by Lépine et al. (see Lépine & Shara 2005; Lépine 2008). The combined IPHAS/UVEX proper motions will have more accurate photometry and better completeness, both because CCD observations are used instead of photographic plates.

(iii) The identification and characterization of open clusters, star-forming regions and (highly reddened) O/B associations down to the magnitude limit of the two surveys.

(iv) The characterization of stellar photometric variability on a 3-year time-scale due to reobservations in the *r* band. This includes the identification of long-period variables (e.g. Mira stars), irregular variables (dwarf novae type cataclysmic variables, soft X-ray transients, flare stars) and a first identification of large amplitude regular variables (e.g. RR Lyrae stars). The EGAPS will also serve as a baseline for new transients in the plane of the Milky Way as shown by our study of Nova Vul 2007 (V458 Vul) whose progenitor was identified in IPHAS data taken only 7 weeks before the nova explosion (Wesson et al. 2008).

In the science goals of the UVEX survey, the *U*-band observations play a crucial role. Since the *U* band is the most sensitive to dust extinction, it is not only a pivotal band to identify those hot but low-luminosity populations in the plane but also a band that will play a very important role in the dust mapping of the plane. Straddling the Balmer jump, it is also the broad-band which is most sensitive to chemical composition and atmospheric pressure in the underlying populations.

3 SURVEY DESIGN AND DATA PROCESSING

Apart from the filters, the survey design is identical to that of the IPHAS as described in D05. The same field centres have been taken, so all fields will be imaged twice in a set of overlapping pointings. The order of field selection for UVEX is mainly based on the availability of 'good' IPHAS data for the same field with a time baseline of at least 3 years. Here, 'good' IPHAS photometry refers to those fields that have a seeing less than 2.0 arcsec, ellipticity of the stellar image <0.2 and a sky background of <2000 cts in *r* (González-Solares et al. 2008). This strategy has been chosen to ensure both a reasonable proper motion baseline and a high-quality data set covering the full optical spectrum. UVEX observations are done in the RGO *U* filter, the Sloan Gunn *g* and *r* filters and the He I 5875 filter. Integration times are 120 s (*U*), 30 s (*g*), 30 s (*r*) and 120/180 s (He I).

Fig. 2 shows the throughput of the *U*, *g*, *r* and He I 5875 filters, as well as the IPHAS *r*, *i* and Hα, overplotted on to the spectrum of Vega. As can be seen in Fig. 2, the He I 5875 filter overlaps with the *r*-band filter, but has a slightly bluer effective wavelength than the *r*

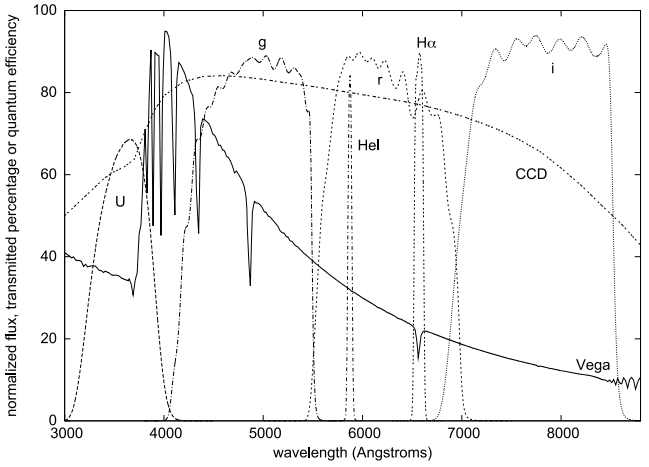

Figure 2. Filter efficiency curves of the U, g, r, He I 5875, Hα and i-band filters used in the UVEX survey and IPHAS (dashed and dash–dotted curves), overplotted on to the spectrum of Vega (solid curve), together with the CCD-efficiency curve (dashed).

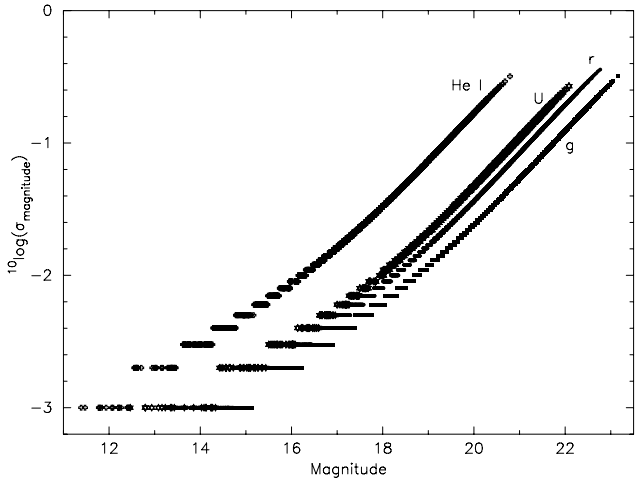

Figure 3. Magnitude errors for the observations in the four different filters as a function of magnitude, as detected in CCD4 of field 6160 taken under median seeing conditions. Note that the He I data are applicable for the 120 s integrations. After the first year, the depth in He I is increased by an enlarged integration time (180 s).

band. For this reason, we construct the (He I $-$ r) colour, adhering to the usual notation for colours to list the bluer band first. Note that the r-band curve is slightly different from that shown in D05, even though it is the same filter. Filter efficiencies were remeasured in 2006 July at the Isaac Newton Group Observatory, resulting in the current efficiency curves.

Data processing is also identical to the IPHAS procedure. All data are transported from the telescope to the Cambridge Astronomy Survey Unit, where it is processed according to the pipeline procedure as detailed in Irwin & Lewis (2001), D05 and González-Solares et al. (2008).

All magnitudes are on the Vega system. The g- and r-band observations are calibrated on a nightly basis by the observation of photometric standards stars from Landolt (1992). Photometric calibration in U, Hα and He I 5875 is hard coupled to that of the g band (for U), and the r-band filter (for Hα and He I 5875). The fixed offsets (in Vega magnitudes) are $U = g - 2.100$, H$\alpha = r - 3.140$ and He I = $r - 3.575$. These shifts have been determined on the basis of spectrophotometric observations combined with the colour modelling discussed in Section 4. On a typical good night, the zero-points (in ADU) for g and r are 25.01 and 24.51, respectively, showing the greater depth of the g-band observations for a given integration time. Since the g- and r-band observations are both 30 s, the g band gives the deepest observations of the combined IPHAS/UVEX survey. A global photometric calibration of both surveys remains to be done.

For illustrative purposes, Fig. 3 shows the magnitude error as a function of magnitude and colour for the UVEX observations of field 6160, where we have taken all data which have been marked as 'stellar' (quality flag '-1' as defined in González-Solares et al. 2008) and on CCD 4 of the wide-field Camera. Fig. 13 shows the colour–magnitude and colour–colour diagrams for the same field.

4 SIMULATION OF THE UVEX COLOUR–COLOUR PLANES

To interpret the UVEX observations, simulations of the colours of stars and the effect of reddening are a very powerful and important tool. In obtaining the simulated colours, we follow the procedure as outlined in D05 for the IPHAS. In short, model and template spectra are folded with the efficiency curves as shown in Fig. 2 and the CCD response curve, and calibrated on the Vega system using equation (1) of D05, where r and i indices should be replaced with the appropriate filter curves. The only difference in this procedure is that we did not rebin all input data to a 5 Å resolution (in D05 set by the resolution of the Pickles 1998, library), but used a fixed 1 Å sampling and a linear interpolation where necessary, as well as an extrapolation on the CCD-efficiency curve on the blue side of the U-band since data were not available. A check on the colours obtained has been made by reproducing the colours as given in D05 for the IPHAS filters (using the filter curves as given in D05). The mean difference and standard deviation on the IPHAS colours derived in D05 and here are $\overline{\Delta(r-i)} = 0.009$ and $\sigma_{(r-i)} = 0.002$ and $\overline{\Delta(r-\mathrm{H}\alpha)} = 0.006$ and $\sigma_{(r-\mathrm{H}\alpha)} = 0.002$. Further checks to the procedure were made by inserting Johnson–Cousins filters into the equation and calculating the colours of main-sequence stars, based on the Pickles spectra, and compared with the colours as given in Bessell (1990) for main-sequence and giant stars and with the Stone & Baldwin (1983) southern spectrophotometric standard stars as given by Landolt (1992).

Our conclusion from these comparisons is that the method accurately reproduces the colours of stars as given in the literature, although there is a large scatter on the ($U - B$) colours. The relatively large scatter with respect to the stars given in Bessell (1990) can also be attributed to the use of a different set of input spectra (the Vilnius spectra used by Bessell versus the Pickles spectra used by us). The comparison with the Baldwin–Stone spectrophotometric standards as given by Landolt (1992) and the colours from D05 show the accuracy of the method. All synthetic colours calculated in this paper are given in the Appendices. The large scatter in the U band is not surprising given its sensitivity to metallicity, atmospheric absorption and the strong variations in detector responses that occur at the bluest wavelengths. This procedure was then used to derive the colours in the UVEX filters, for normal stars (luminosity classes V, III and I), emission-line objects and white dwarfs. See Tables A1–A6 in the Appendix.

Based on the colour simulations presented below, and also folding the Pickles spectra with standard Johnson–Cousins filter curves, we derive the following colour transformations from Johnson–Cousins

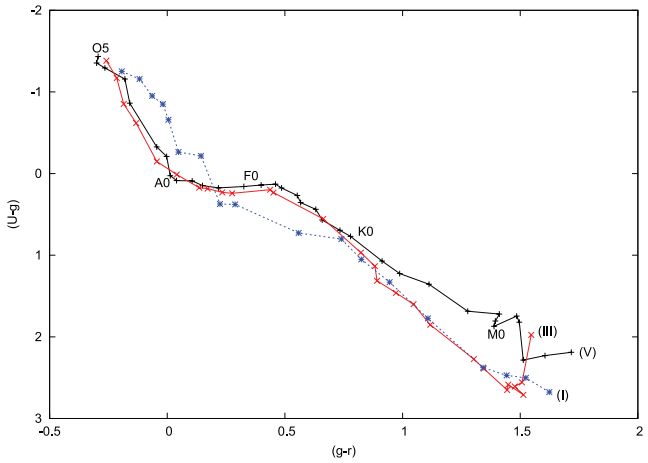

Figure 4. Simulated colours of main-sequence (V, black), giant (III, red) and supergiant (I, blue) stars in the UVEX $(U - g)$ versus $(g - r)$ plane.

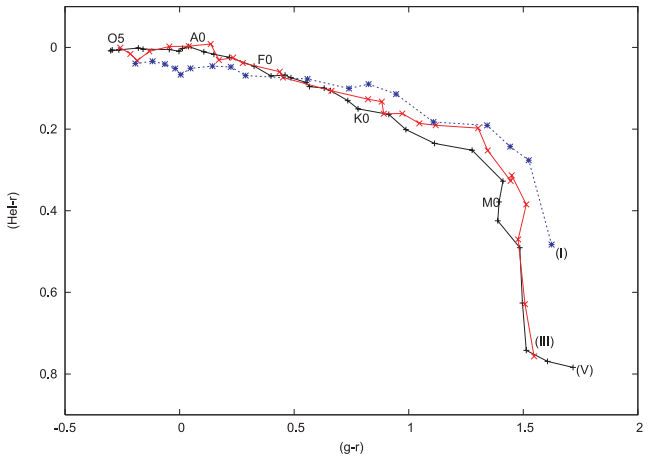

Figure 5. Simulated colours of main-sequence (V, black), giant (III, red) and supergiant (I, blue) stars in the UVEX (He I $- r$) versus $(g - r)$ plane.

to the IPHAS/UVEX colour space:

$$(U - g) = 1.035\,(U - B) + 0.470\,(B - V) - 0.017, \quad (1)$$

$$(g - r) = 1.044\,(B - V) - 0.116\,(V - R) + 0.025, \quad (2)$$

$$(r - i) = 1.484\,(R - I) - 0.389\,(V - R) - 0.014. \quad (3)$$

These transformations are valid over the colour region of $-1.43 < (U - g) < 2.19$, $-0.30 < (g - r) < 1.72$ and $-0.17 < (r - i) < 2.58$. Please note that all magnitudes here are on the Vega system. Transferring to the AB system can be done by using the relations given on the Astronomy Survey Unit's webpage.[1]

4.1 UVEX colours of main-sequence, giant and supergiant stars

To simulate the colours of normal stars with luminosity classes V (main-sequence dwarfs), III (giants) and I (supergiants) we make use of the Pickles (1998) library. After application of the procedure outlined above, the results are shown in Figs 4 and 5 and are tabulated in Appendix A. Here, we use the $(g - r)$ versus $(U - g)$ and the $(g - r)$ versus (He I $- r$) colour–colour diagrams as our fundamental planes. It can be seen that the difference in colours between main-sequence stars, giants and supergiants is relatively small and all objects are restricted to a narrow band. In the $(g - r)$ versus (He I$-r$) plane, a characteristic 'hook' is displayed, appearing around M0, after which the stars show a distinct increase in the (He I$- r$) colour, caused by the appearance of strong TiO absorption bands depressing the flux in the He I band.

[1] http://www.ast.cam.ac.uk/~wfcsur/technical/photom/colours/

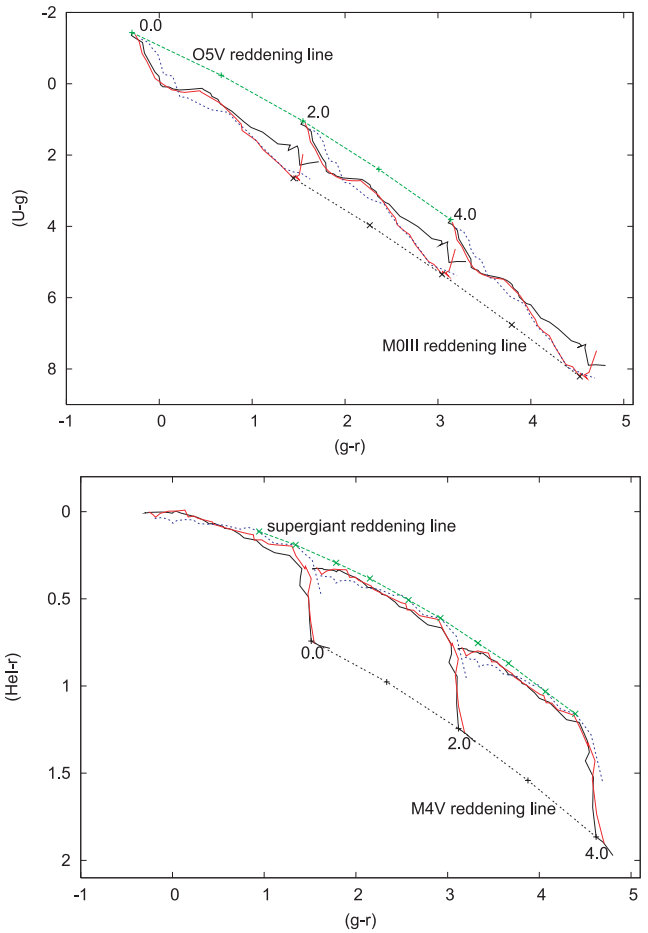

Figure 6. Synthetic colour–colour diagrams in the UVEX filter system for main sequences, giant and supergiant, using the reddening law of Cardelli et al. (1989). Colours are shown for $E(B - V) = 0.0$, 2.0 and 4.0. Also shown are the encompassing upper and lower envelope curves: the O5V and the M0III reddening curves.

To simulate the effect of reddening, we have applied the extinction laws of Cardelli, Clayton & Mathis (1989), with a fixed $R = 3.1$. Results are shown in Fig. 6. Template and model spectra were first multiplied by the extinction laws and then folded through the filter curves. It is clear from Fig. 6 that, in analogy to the IPHAS colours, also here envelope lines exist, indicating a limit above/underneath which no normal main-sequence stars, giants or supergiants are expected. In Fig. 6, these are indicated with 'O5V-reddening' line and 'M0III reddening line'.

4.2 Colours of helium emission-line stars

The inclusion of the He I 5875 filter has been made to enable the detection of strong He I 5875 absorbers (e.g. DB-type white dwarfs) or emitters [e.g. AM CVn stars and cataclysmic variables]. Again,

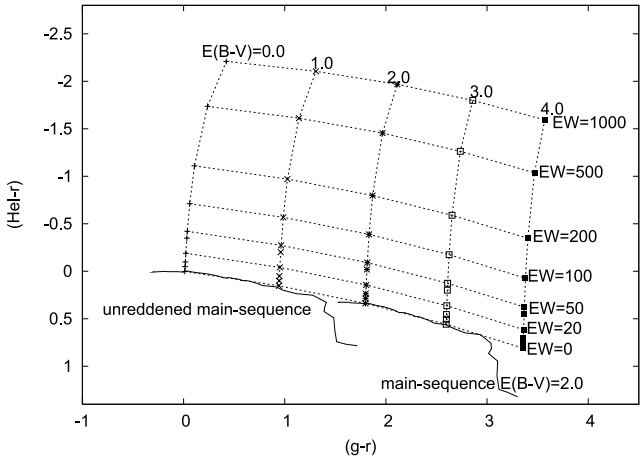

Figure 7. Position of He I 5875 emission-line objects in the $(g - r)$ versus (He I $- r$) colour space. Horizontal lines mark objects of equal EWs in units of Å, vertical lines mark lines of constant reddening, assuming an underlying A0V spectrum.

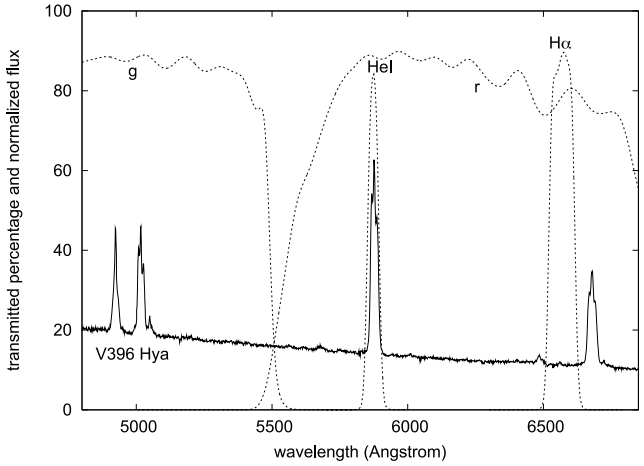

Figure 8. Spectrum of the AM CVn star V396 Hya (Ruiz et al. 2001), overplotted with the UVEX/IPHAS narrow-band filter curves of He I 5875 and Hα and the broad-band g and r bands.

in analogy with D05 we have determined the sensitivity to pick out He I emission using an A0V underlying continuum (very similar to a power-law slope with index –3) to which an emission line is added. The emission line is simulated by a top-hat-shaped line having a width that is equal to the full width at half-maximum (FWHM) of the He I filter, 40Å. The results are shown in Fig. 7. Reddening has been added to these data in discrete steps of 1 from $E(B - V) = 0$ to 4. Overplotted on to the grid of emission-line strength is the unreddened main sequence as determined in Section 4.1. It can be seen from Fig. 7 that emission strength above already a few Å should stand out in UVEX observations, depending mostly on the photometric accuracy of the observations. This is only marginally influenced by reddening due to the narrowness of the He I filter and its position within the r band. A similar behaviour is seen in the $(r - \mathrm{H}\alpha)$ colour although the effect is larger there (D05).

4.3 The colours of AM Canum Venaticorum stars

AM CVn stars are hydrogen-depleted, short-period interacting binaries consisting of a white dwarf primary and a white dwarf or semidegenerate helium star secondary, sometimes also called 'helium cataclysmic variables' (see e.g. Nelemans 2005 for an overview). These systems show orbital periods in the range $5.4 < P_{\mathrm{orb}} < 65$ min. At longer orbital periods ($P_{\mathrm{orb}} \gtrsim 30$ min), their spectra are dominated by strong helium emission lines (see e.g. Marsh, Horne & Rosen 1991; Roelofs et al. 2005, 2006a,b). The strongest of these lines is the He I 5875 line. Fig. 8 shows the spectrum of V396 Hya (Ruiz et al. 2001) with the UVEX/IPHAS narrow-band filters of He I 5875 and Hα overplotted. It can be seen that the He I 5875 filter width exactly matches the width of the emission line and therefore provides maximum sensitivity to these systems.

Using the publicly available Sloan spectra and the Very Large Telescope (VLT) spectra as presented in Roelofs et al. (2005, 2006a, 2007b,c), we constructed a $(g - r)$ versus (He I $- r$) colour–colour diagram of long-period AM CVn stars (Fig. 9). It can be seen that indeed the long-period AM CVn stars lie significantly above the main sequence in (He I $- r$) due to their He I 5875 emission. The vertical spread of the AM CVn systems indicates increasing He I equivalent widths (EWs) at almost constant broad-band colours.

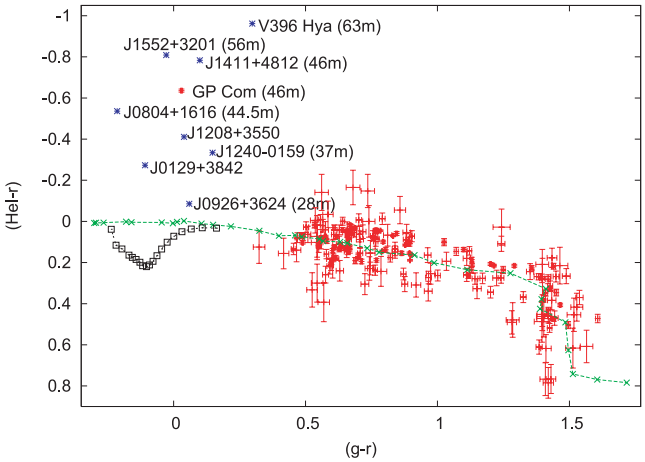

Figure 9. Position of AM CVn stars in a $(g - r)$ versus (He I $- r$) colour–colour diagram. Asterisks show the position of known AM CVn stars, based on their SDSS spectrum. Labels refer to the AM CVn stars and, if known, the orbital period is added (see Roelofs et al. 2009 for SDSS J0804). The AM CVn points are overlaid on to the UVEX colours of stars in the field of GP Com (red symbols), which itself is shown by the (red) point at $(g - r) = 0.05$ and (He I $- r$) $= -0.65$. Also shown is the unreddened main sequence as the green dashed line marked by crosses, and the DB sequence as the purple dotted line marked with squares.

4.4 Simulation of DA and DB white dwarfs

As uncovering the population of single and binary white dwarfs at low Galactic latitude is one of the main goals of the UVEX survey, we have also simulated the expected colours of a set of white dwarfs. These simulations are based on two sets of white dwarf model spectra available to us: one set kindly provided by D. Koester, spanning the temperature range 6000–80 000 K and surface gravity range $\log g = 7.0$–9.0, for both hydrogen-dominated atmospheres (DA white dwarfs) and helium-dominated atmospheres (DB white dwarfs) and one set kindly provided by P. Bergeron spanning the temperature range 1500–17 000 K and surface gravity range $\log g = 7.0$–9.0, for hydrogen-dominated atmospheres (DA white dwarfs). In the coolest models ($T < 4000$ K), the effect of collisional induced absorption due to the formation of H_2 was included. See Finley, Koester & Basri (1997), Koester et al. (2001) and Bergeron,

Wesemael & Beauchamp (1995) for details on the calculation of these models. Both sets of models were provided on a non-linear wavelength grid, where the lines were more densely sampled than the continuum region. Both sets of models were interpolated on a regular grid with a 1 Å binning, identical to the sampling of the filter curves and CCD efficiency. In the overlapping region, both sets of models were compared with each other, and were found to be identical on the level of <2 per cent at all wavelengths with the exception of the very cores of the lines, where differences can increase to ∼4 per cent over a small wavelength range.

For the calculation of the white dwarf models, we have used the models with a fixed surface gravity of log $g = 8.0$. Fig. 10 shows the colours of the white dwarf models in the UVEX colour–colour planes.

4.5 Simulations of cataclysmic variables

The location of cataclysmic variables in Hα narrow-band surveys has been extensively discussed in Witham et al. (2006). In the IPHAS, based on solely the $r - H\alpha$ and $r - i$ colours, it is difficult to make a photometric distinction between highly reddened background early-type emission-line objects and cataclysmic variables. With the addition of the UVEX colours, this will become easier. Cataclysmic variables are intrinsically rather faint ($M_V \gtrsim 5$) but blue, making them on average much less reddened than intrinsically brighter objects at the same colour. We have simulated the position of cataclysmic variables in the UVEX survey by taking the sample of SDSS cataclysmic variables (Szkody et al. 2002, 2003, 2004, 2005, 2006, 2007) and folded them through the UVEX filter curves. The U-band magnitude could not be calculated due to the blue cut-off in the Sloan spectra at $\lambda \sim 3800$ Å. In Fig. 11, we show the colour of all SDSS cataclysmic variables and AM CVn stars in the UVEX/IPHAS colour planes.

5 COMPARISON WITH OBSERVED DATA

Data taking for UVEX had started in the summer of 2006, and up to 2008 September 30 per cent had been observed. After quality control checks, all data will be made public through the web site of the EGAPS.[2]

5.1 Control fields and survey depth

To check our photometric calibration and extraction algorithms in highly crowded areas, a number of globular clusters were observed as control fields. In Fig. 12, we show the colour–magnitude and colour–colour diagrams for NGC 5904, overlaid with our main-sequence colour tracks. It is clear from Fig. 12 that the extraction mechanism works very well, even in severely crowded regions. The limiting magnitude, defined here as the magnitude where the magnitude error reaches 0.2 mag (i.e. $\sim 5\sigma$, which would be an error of 0.22 mag), of UVEX data under good conditions (r-band seeing of 1.1 arcsec) is 21.8 (U), 22.6 (g), 22.1 (r) and 20.2 (He I 5875). A limiting magnitude set at 0.2 mag error in the magnitude value encompasses between 95 and 98 per cent of all stellar objects, depending on the filter. Part of the He I 5875 observations is taken with 180 s integration, increasing the limiting magnitude. In general, of course, the limiting magnitude of each individual exposure will depend on seeing, transparency, sky brightness and, in severe cases, also crowding (see Section 6).

[2] www.egaps.org, see also www.iphas.org.

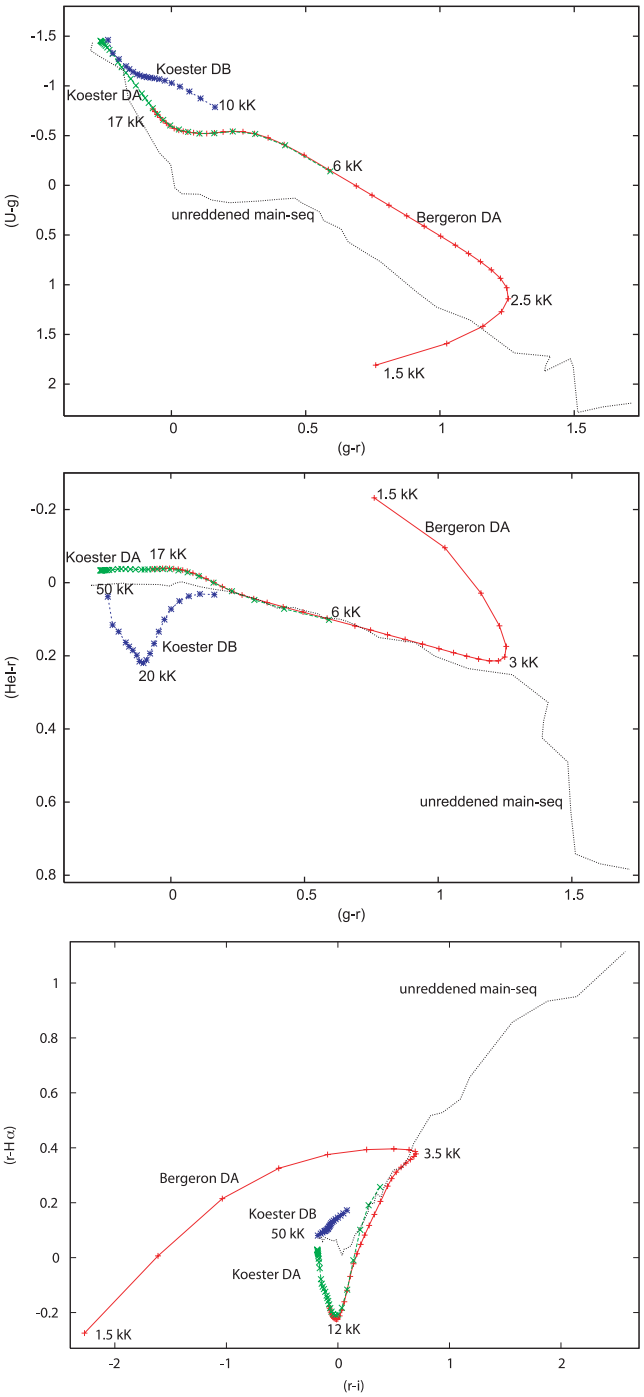

Figure 10. Top panel: position of log $g = 8.0$ DA and DB white dwarf in the UVEX ($g - r$) versus ($U - g$) colour–colour plane based on the Bergeron models (DA) and Koester models (DA and DB) for temperature between 1500 and 80 000 K (DA) and 10 000–50 000 K (DB). DB models with temperature <10 000 K are identical to blackbodies. The characteristic 'hook' in the DA models between temperature 7000 and 25 000 K is due to the Balmer jump which lies in the U band. The hook at $T \lesssim 2500$ K is due to collisionally induced absorption by the H_2 molecule. Middle panel: same models as in the previous panel in the ($g - r$) versus (He I $- r$) colour plane. The DA models with $T > 3000$ K virtually overlie the main-sequence models shown in Fig. 5. The DB models show a pronounced reddening of the He I $- r$ colour due to the He absorption line at He I 5875. Bottom panel: same models as in the previous panels in the ($r - i$) versus ($r - H\alpha$) colour, to show the distinction that can be made in these colours between DA and non-DA white dwarfs based on the deep Hα absorption.

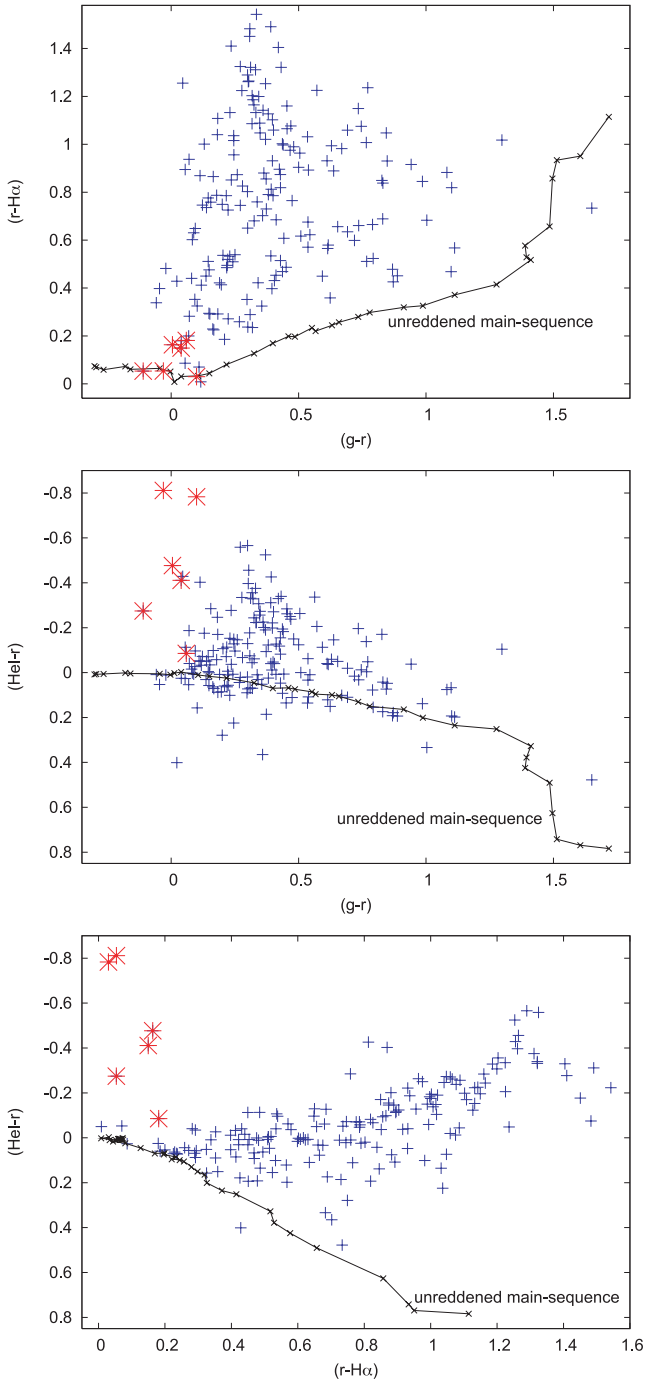

Figure 11. UVEX/IPHAS colour–colour diagram of all currently known Sloan cataclysmic variables ('+' signs) and AM CVn stars ('*' signs) in $(g-r)$ versus $(R-\mathrm{H}\alpha)$ (top panel), $(g-r)$ versus $\mathrm{He\,I}-r$ (middle panel) and $(r-\mathrm{H}\alpha)$ versus $(\mathrm{He\,I}-r)$ (bottom panel), together with the unreddened main-sequence track.

5.2 Galactic plane data

In Figs 13 and 14, we show two representative fields from the Galactic plane centred on $(l, b = 79.^{\circ}6, -2.^{\circ}8)$ and $(l, b = 83.^{\circ}0, -0.^{\circ}1)$, respectively. In the extraction, only sources with quality flag '−1' (stellar) and '−2' (probably stellar) have been taken into account, and the condition was set that the sources were detected in both the direct and the offset fields. In the colour–colour diagrams, we overplot the colour tracks for unreddened data as well as for $E(B-V) = 2.0$ and 4.0.

In field 6160 (Fig. 13, $l = 79.^{\circ}6$, $b = -2.^{\circ}8$), it can be clearly seen that the main-sequence stars are reddened [$E(B-V) = 1.25$ according to Schlegel, Finkbeiner & Davis 1998]. On the blue side, a small number of blue excess sources are present, varying in magnitude between $18.5 < g < 22.5$ and at $g - r \sim 0$. These are unreddened, intrinsically blue and intrinsically low-luminosity objects that lie in front of the bulk of the main-sequence population. These are the 'UV-Excess' sources that give their name to the survey: predominantly white dwarfs and white dwarf binaries. The reddening of the main-sequence causes the bulk of the stars to shift to redder colours overall, uncovering a population of 'warm' ($T < 10\,000$ K) white dwarfs. In unreddened (higher galactic latitude) fields, these 'warm' white dwarfs merge with the main sequence and become difficult to identify in broad-band photometry. Due to the shallower depth of the He I observations, the faintest UV-Excess sources in g are not detected in the He I filter (Fig. 13). Due to their blue colour, most are detected in the U band. A distinction between DA and DB white dwarfs can already be made on the basis of the $(U-g)$ versus $(g-r)$ diagram, but will be further aided by the $(\mathrm{He\,I}-r)$ versus $(g-r)$ and the $(\mathrm{He\,I}-r)$ versus $(r-\mathrm{H}\alpha)$ diagrams.

In field 6167 (Fig. 14), the reddening is higher [$E(B-V) = 3.10$ according to Schlegel et al. 1998], which is not surprising given its location in the mid-plane. The reddening is such that all stars earlier than M0 are substantially reddened. In the $(\mathrm{He\,I}-r)$ versus $(g-r)$ diagram, M-type stars show a distinctive downturn in the $\mathrm{He\,I}-r$ colour, making them easily identifiable. The same stars can be seen as the almost vertical sequence at $g - r = 1.5$ and running from $19 < g < 23$. Counterintuitively, the intrinsically faint late-type M stars have become some of the *bluest* objects in the field, apart from the real stellar remnants located bluewards of $g - r < 1$ and $g > 19$.

6 SEEING STATISTICS AND CROWDING

For all data up to 2007 November, we have collected the seeing statistics in the four UVEX filters (Fig. 15). This is for a total of ∼375 deg^2 and ∼3000 pointings over the period 2006 June–2007 November. It can be seen from Fig. 15 that the median seeing in the UVEX data so far is (1.3, 1.1, 1.0, 1.4 arcsec) for the (U, g, r, He I) filters, respectively. The He I data show a qualitatively different behaviour than the other three bands with a much broader maximum. This is most likely caused by the fact that most of the He I data are taken with an integration time of 180 s, but with no autoguider. This causes small errors in the telescope tracking, which translate into a deteriorated seeing.

With the stellar densities expected and detected in the Galactic plane down to $g \sim 22$, crowding becomes a real concern for number statistics studies. Surface densities of detected point sources in the UVEX fields can reach up to 200 000 sources per pointing, i.e. 700 000 stars deg^{-2}. Following Irwin & Trimble (1984), we here make a global estimate of the effect of crowding in the UVEX data. Using their equation (4) and inserting the relevant numbers for UVEX, we calculate the crowding correction factor (i.e. their f'/f) for seeing disc FWHM values of 0.7–1.2 arcsec as shown in Fig. 16. As can be seen, the crowding factor is a strong function of the actual seeing, and also of the assumed radius of the actual stellar profile. Fig. 16 shows the correction factors for both a 2σ Gaussian profile cut-off radius and a 3σ cut-off. We see that at the maximum density of detected sources in UVEX, which is close to 1 million

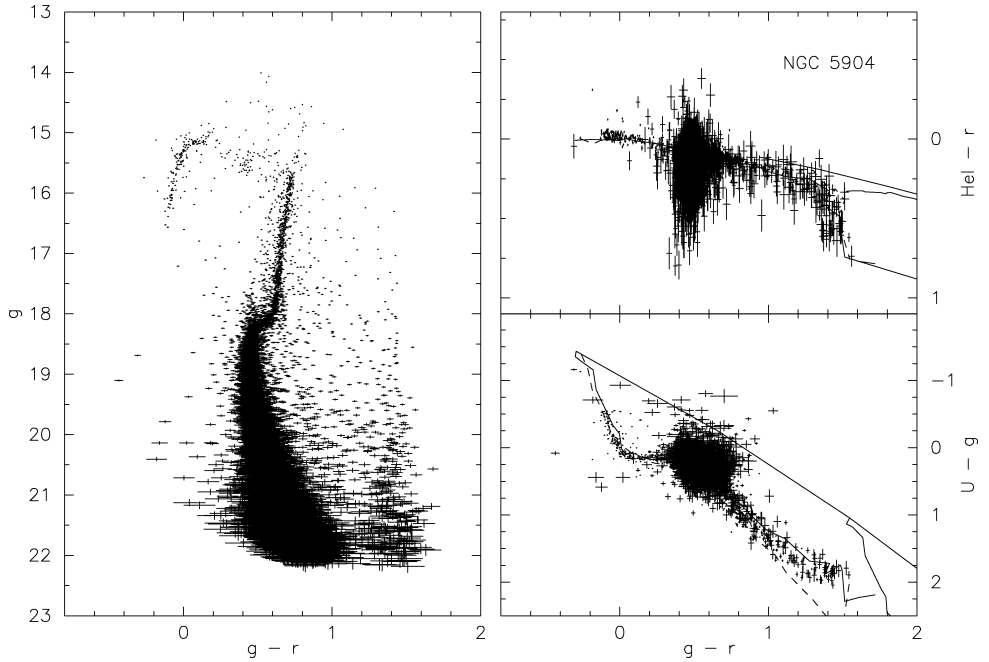

Figure 12. Colour–colour and colour–magnitude diagrams of globular cluster NGC 5904 (M5), showing all detected objects with a magnitude error <0.1 for clarity, overlaid in the colour–colour diagrams with the UVEX colour tracks as presented in Section 4. Full lines are for main-sequence stars and dashed lines for giants. The O5-reddening line and the supergiant reddening lines are also shown as the upper and lower envelopes (see Fig. 6)

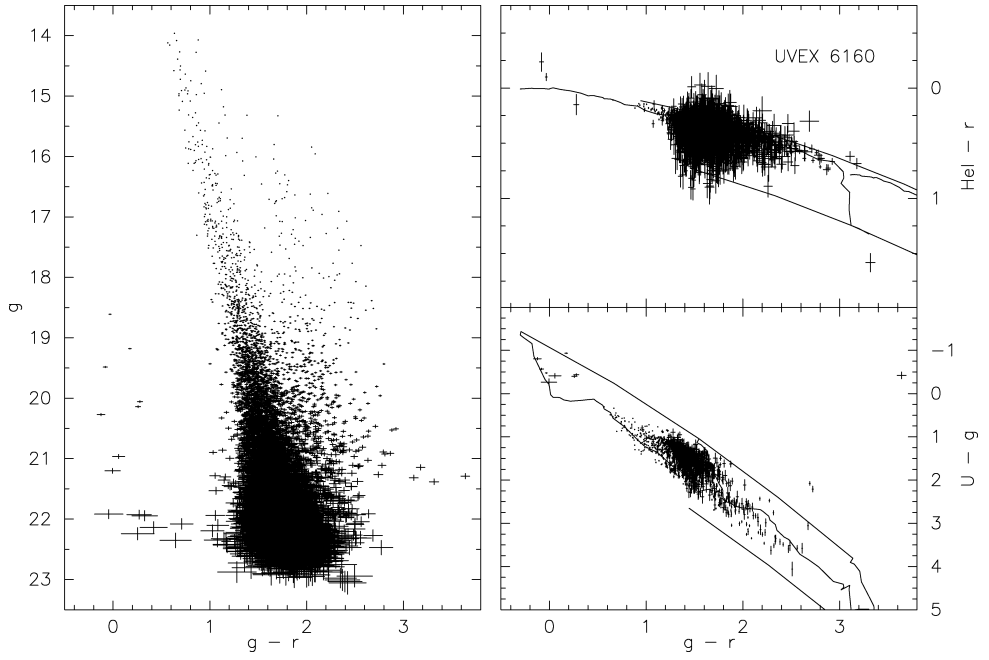

Figure 13. Colour–colour and colour–magnitude diagrams of field 6160, showing all detected objects with a magnitude error <0.1 for clarity, overlaid in the colour–colour diagrams with the UVEX colour tracks as presented in Section 4.

sources per square degree, we reach a crowding correction of at least 20 per cent in the best of cases (0.7 arcsec seeing, 2σ cut-off) and quickly reach >100 per cent when a 3σ cut-off radius is taken. Of course in reality the actual crowding will also depend on the actual magnitude difference between two nearby, almost overlapping sources and will require a detailed field-to-field modelling, but this global estimate shows that for the most crowded regions of the Galactic plane crowding is a serious issue.

7 CONCLUSIONS

The UVEX survey offers the possibility to detect intrinsically blue, faint objects in the Galactic plane, as well as offers the first-ever homogeneous blue survey of the Galactic plane and is ideal for uncovering a large population of stellar remnants. The depth of the *g*-band observations, close to the ground-based confusion limit, will allow for detailed Galactic structure research. The combination

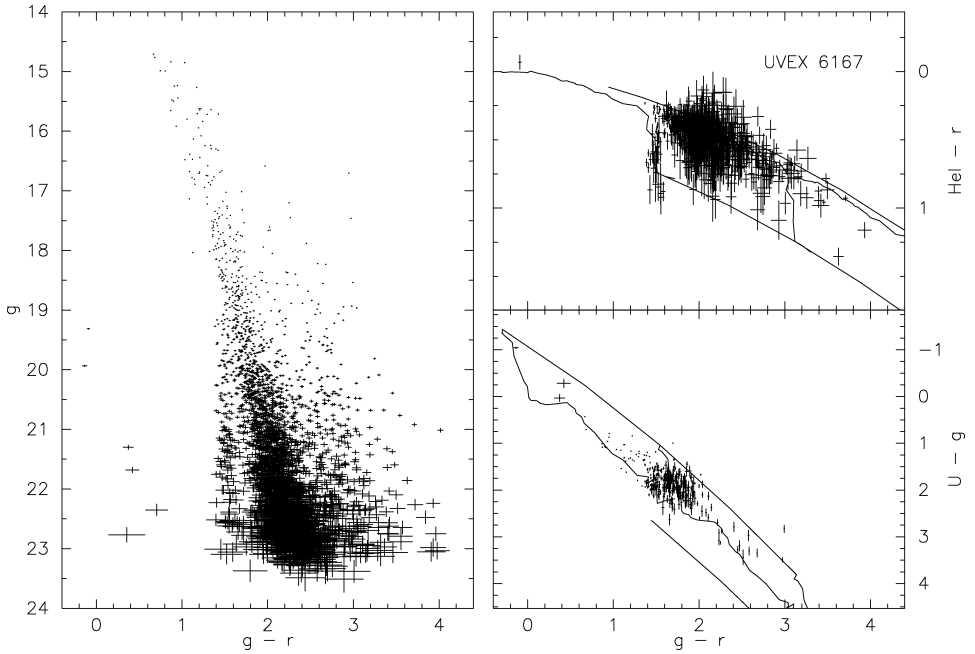

Figure 14. Colour–colour and colour–magnitude diagrams of field 6167, showing all detected objects with a magnitude error <0.1 for clarity, overlaid in the colour–colour diagrams with the UVEX colour tracks as presented in Section 4.

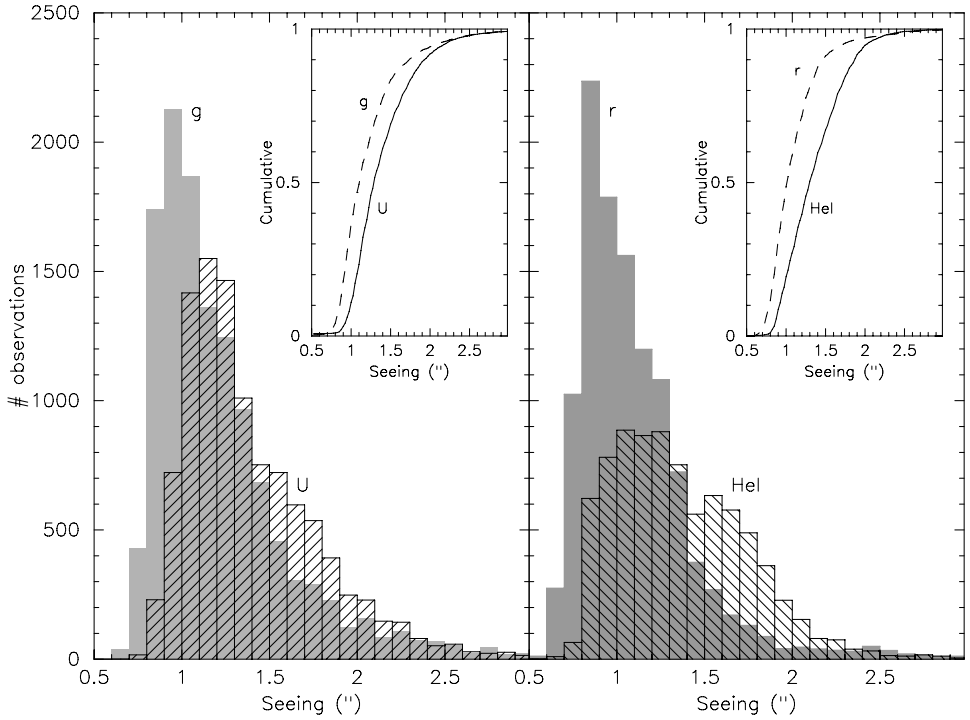

Figure 15. Seeing distributions for UVEX observations in the period 2006 June–2007 November, for the *U*- and *g*-band observations (left-hand panel) and the *r*- and He I-band observations (right-hand panel). Insets show the cumulative distributions.

with the IPHAS offers the first-ever optical survey of the northern Galactic plane in the U, g, r, i, Hα and He I 5875 filters. The southern plane will be covered by the VPHAS+ survey in the same bands (minus the He I band), on the VLT Survey Telescope at the ESO. Combined these three surveys form the heart of the EGAPS. When completed, the EGAPS will provide positions, colours for close to 1 billion stars in our Galaxy. From the first study on proper motions from the EGAPS, Deacon et al. (2009) showed that we can expect ∼140 objects per square degree with a proper motion $\mu \geq 20$ mas yr^{-1}.

ACKNOWLEDGMENT

This paper makes use of the data collected at the Isaac Newton Telescope, operated on the island of La Palma by the Isaac Newton Group in the Spanish Observatorio del Roque de los Muchachos

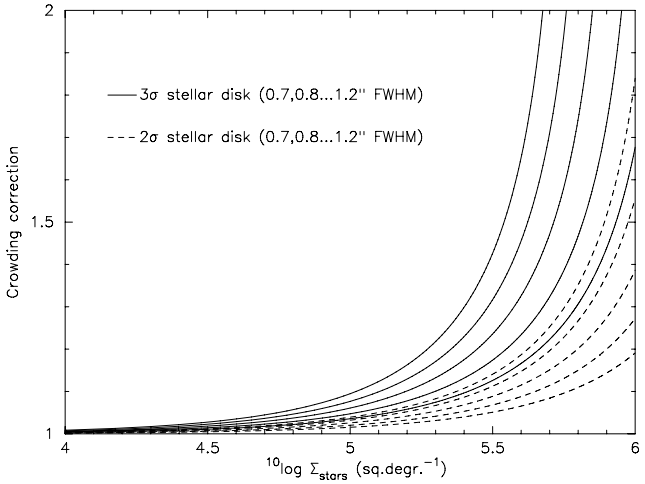

Figure 16. Crowding correction factor (f'/f in equation 4 of Irwin & Trimble 1984) between observed versus actual number densities of stars for a range in seeing FWHMs (0.7, 0.8, . . . ,1.2: lines from bottom to top, respectively) and for two settings of the stellar image threshold radius at 2σ (dashed lines) and 3σ (full lines) Gaussian e-folding lengths.

of the Instítuto de Astrofísica de Canarias. We acknowledge the use of data products from Two-Micron All-Sky Survey, which is a joint project of the University of Massachusetts and the Infrared Processing and Analysis Center/California Institute of Technology (funded by the National Aeronautics and Space Administration and National Science Foundation of the USA). KV is supported by an NWO-EW grant 614.000.601 to PJG. ND is supported by NOVA and NWO-VIDI grant 639.042.201 to PJG. The authors would like to thank Detlev Koester and Pierre Bergeron for making available their white dwarf models on which a significant part of the colour simulations in this paper is based.

REFERENCES

Bergeron P., Wesemael F., Beauchamp A., 1995, PASP, 107, 1047
Bessell M. S., 1990, PASP, 102, 1181
Boissier S., Prantzos N., 1999, MNRAS, 307, 857
Cardelli J. A., Clayton G. C., Mathis J. S., 1989, ApJ, 345, 245
Deacon N. et al., 2009, MNRAS, in press (arXiv:0905.2594)
Drew J. et al., 2005, MNRAS, 362, 753 (D05)
Drew J., Greimel R., Irwin M. J., Sale S. E., 2008, MNRAS, 386, 1761
Finley D. S., Koester D., Basri G., 1997, ApJ, 488, 375
González-Solares E. A. et al., 2008, MNRAS, 388, 89
Irwin M., Lewis J., 2001, New Astron., 45, 105
Irwin M., Trimble V., 1984, AJ, 89, 83
Koester D. et al., 2001, A&A, 378, 556
Landolt A., 1992, AJ, 104, 340
Lanning H. H., 1973, PASP, 85, 70
Lanning H. H., Lépine S., 2006, PASP, 118, 1639
Lanning H. H., Meakes M., 2004, PASP, 116, 1039
Lépine S., 2008, AJ, 135, 2177
Lépine S., Shara M. M., 2005, AJ, 129, 1483
Marsh T. R., Horne K., Rosen S., 1991, ApJ, 366, 535
Nelemans G., 2005, in Hameury J.-M., Lasota J.-P., eds, ASP Conf. Ser., Vol. 330, The Astrophysics of Cataclysmic Variables and Related Objects. Astron. Soc. Pac., San Francisco, p. 27
Nelemans G., Jonker P. G., Marsh T. R., Van der Klis M., 2004a, MNRAS, 348, L7
Nelemans G., Yungelson L. R., Portegies Zwart S. F., 2004b, MNRAS, 349, 181
Pickles A. J., 1998, PASP, 110, 863
Roelofs G. H. A., Groot P. J., Marsh T. R., Steeghs D., Barros S. C. C., Nelemans G., 2005, MNRAS, 361, 487
Roelofs G. H. A., Groot P. J., Marsh T. R., Steeghs D., Nelemans G., 2006a, MNRAS, 365, 1109
Roelofs G. H. A., Groot P. J., Marsh T. R., Steeghs D., Nelemans G., 2006b, MNRAS, 371, 1231
Roelofs G. H. A., Nelemans G., Groot P. J., 2007a, MNRAS, 382, 685
Roelofs G. H. A., Groot P. J., Nelemans G., Marsh T. R., Sleeghs D., 2007b, MNRAS, 379, 176
Roelofs G. H. A., Groot P. J., Sleeghs D., Marsh T. R., Nelemans G., 2007c, MNRAS, 382, 1643
Roelofs G. H. A. et al., 2009, MNRAS, 394, 367
Ruiz M. T., Rojo P. M., Garay G., Maza J., 2001, ApJ, 552, 679
Sale S. et al., 2009, MNRAS, 392, 497
Sandage A., 1972, ApJ, 178, 1
Schlegel D. J., Finkbeiner D. P., Davis M., 1998, ApJ, 500, 525
Steinmetz M. et al., 2006, AJ, 132, 1645
Stone R. P. S., Baldwin J. A., 1983, MNRAS, 204, 347
Szkody P. et al., 2002, AJ, 123, 430
Szkody P. et al., 2003, AJ, 126, 1499
Szkody P. et al., 2004, AJ, 128, 1882
Szkody P. et al., 2005, AJ, 129, 2386
Szkody P. et al., 2006, AJ, 131, 973
Szkody P. et al., 2007, AJ, 134, 185
Wesson R. et al., 2008, ApJ, 688, L21
Witham A. R. et al., 2006, MNRAS, 369, 581
Yanny B. et al., 2009, AJ, 137, 4377
York D. G. et al., 2000, AJ, 120, 1579

APPENDIX A: UVEX COLOURS FOR MAIN-SEQUENCE STARS, INCLUDING REDDENING

Table A1. UVEX colour indices $(U-g)$, $(g-r)$, (He I $-r$) for Pickles main-sequence stars including reddening.

Spectral	$E(B-V)=0.0$			$E(B-V)=1.0$			$E(B-V)=2.0$			$E(B-V)=3.0$			$E(B-V)=4.0$		
type	$U-g$	$g-r$	He I $-r$	$U-g$	$g-r$	He I $-r$	$U-g$	$g-r$	He I $-r$	$U-g$	$g-r$	He I $-r$	$U-g$	$g-r$	He I $-r$
O5V	−1.434	−0.294	0.006	−0.239	0.667	0.149	1.044	1.547	0.326	2.400	2.364	0.538	3.811	3.137	0.784
O9V	−1.355	−0.301	0.008	−0.153	0.652	0.151	1.134	1.525	0.329	2.492	2.338	0.541	3.903	3.111	0.788
B0V	−1.293	−0.265	0.006	−0.099	0.691	0.148	1.183	1.567	0.326	2.537	2.381	0.538	3.945	3.152	0.784
B1V	−1.158	−0.180	0.001	0.047	0.767	0.146	1.337	1.635	0.326	2.699	2.442	0.541	4.111	3.209	0.788
B3V	−0.863	−0.160	0.004	0.331	0.785	0.151	1.609	1.651	0.332	2.956	2.458	0.548	4.354	3.226	0.798
B8V	−0.327	−0.045	0.005	0.842	0.895	0.153	2.095	1.757	0.337	3.418	2.561	0.555	4.792	3.326	0.806
B9V	−0.210	−0.003	0.009	0.961	0.932	0.160	2.217	1.791	0.345	3.542	2.592	0.564	4.918	3.355	0.816
A0V	0.026	0.013	0.002	1.196	0.943	0.153	2.451	1.798	0.338	3.775	2.596	0.558	5.149	3.357	0.811
A2V	0.085	0.039	−0.002	1.253	0.969	0.149	2.504	1.823	0.336	3.824	2.621	0.557	5.194	3.383	0.812
A3V	0.090	0.106	0.011	1.267	1.029	0.164	2.528	1.878	0.352	3.856	2.672	0.575	5.233	3.431	0.831
A5V	0.148	0.150	0.017	1.329	1.066	0.171	2.594	1.909	0.361	3.926	2.698	0.585	5.305	3.454	0.842
A7V	0.175	0.217	0.024	1.367	1.134	0.182	2.641	1.978	0.374	3.981	2.769	0.600	5.368	3.526	0.859
F0V	0.158	0.325	0.046	1.370	1.235	0.208	2.662	2.074	0.405	4.017	2.862	0.637	5.416	3.618	0.901
F2V	0.140	0.399	0.070	1.365	1.299	0.235	2.669	2.131	0.435	4.035	2.914	0.669	5.444	3.667	0.935
F5V	0.130	0.460	0.068	1.369	1.355	0.234	2.685	2.182	0.436	4.062	2.962	0.670	5.482	3.713	0.937
F6V	0.177	0.486	0.074	1.416	1.382	0.242	2.732	2.212	0.445	4.109	2.994	0.682	5.529	3.747	0.951
F8V	0.269	0.552	0.086	1.514	1.443	0.256	2.836	2.268	0.462	4.217	3.047	0.701	5.640	3.798	0.971
G0V	0.355	0.567	0.096	1.602	1.455	0.268	2.925	2.280	0.474	4.307	3.060	0.714	5.731	3.811	0.985
G2V	0.438	0.631	0.100	1.695	1.514	0.273	3.028	2.335	0.481	4.417	3.112	0.722	5.847	3.862	0.995
G5V	0.569	0.658	0.106	1.829	1.536	0.280	3.162	2.353	0.489	4.552	3.127	0.732	5.983	3.875	1.005
G8V	0.695	0.734	0.130	1.972	1.610	0.307	3.319	2.427	0.519	4.721	3.202	0.764	6.162	3.951	1.040
K0V	0.769	0.779	0.150	2.036	1.656	0.331	3.376	2.474	0.545	4.771	3.250	0.793	6.204	4.000	1.071
K2V	1.072	0.913	0.164	2.360	1.780	0.346	3.717	2.591	0.563	5.126	3.361	0.813	6.572	4.107	1.093
K3V	1.225	0.988	0.201	2.498	1.864	0.387	3.844	2.681	0.607	5.246	3.454	0.859	6.688	4.201	1.143
K4V	1.356	1.113	0.235	2.648	1.976	0.425	4.009	2.784	0.649	5.424	3.553	0.906	6.877	4.297	1.193
K5V	1.686	1.277	0.252	2.983	2.133	0.443	4.346	2.935	0.667	5.760	3.698	0.923	7.210	4.436	1.209
K7V	1.721	1.411	0.328	3.032	2.250	0.526	4.407	3.038	0.758	5.831	3.791	1.021	7.288	4.522	1.313
M0V	1.806	1.394	0.378	3.109	2.245	0.580	4.478	3.044	0.816	5.895	3.806	1.083	7.347	4.545	1.379
M1V	1.872	1.389	0.425	3.174	2.227	0.628	4.541	3.015	0.865	5.956	3.768	1.133	7.404	4.501	1.430
M2V	1.745	1.485	0.491	3.059	2.320	0.702	4.436	3.105	0.946	5.859	3.857	1.220	7.313	4.590	1.523
M3V	1.821	1.496	0.626	3.143	2.320	0.848	4.525	3.098	1.102	5.949	3.848	1.386	7.401	4.581	1.697
M4V	2.285	1.513	0.742	3.622	2.336	0.977	5.013	3.119	1.244	6.442	3.876	1.542	7.895	4.619	1.866
M5V	2.230	1.605	0.769	3.583	2.423	1.006	4.986	3.202	1.275	6.423	3.956	1.573	7.883	4.696	1.896
M6V	2.189	1.717	0.784	3.568	2.526	1.038	4.988	3.302	1.323	6.437	4.059	1.635	7.904	4.803	1.972

Table A2. UVEX colour indices $(U-g)$, $(g-r)$, (He I $-r$) for Pickles giants including reddening.

Spectral	$E(B-V)=0.0$			$E(B-V)=1.0$			$E(B-V)=2.0$			$E(B-V)=3.0$			$E(B-V)=4.0$		
type	$U-g$	$g-r$	He I $-r$	$U-g$	$g-r$	He I $-r$	$U-g$	$g-r$	He I $-r$	$U-g$	$g-r$	He I $-r$	$U-g$	$g-r$	He I $-r$
O8III	−1.382	−0.259	0.001	−0.181	0.696	0.143	1.107	1.571	0.320	2.468	2.383	0.532	3.881	3.154	0.777
B1-2III	−1.170	−0.215	0.016	0.029	0.733	0.160	1.315	1.603	0.340	2.671	2.412	0.554	4.078	3.181	0.801
B3III	−0.852	−0.185	0.032	0.344	0.759	0.179	1.626	1.627	0.361	2.976	2.435	0.578	4.378	3.204	0.828
B5III	−0.619	−0.132	0.010	0.568	0.812	0.158	1.838	1.679	0.341	3.178	2.487	0.559	4.568	3.256	0.810
B9III	−0.148	−0.045	−0.002	1.012	0.895	0.147	2.256	1.757	0.330	3.571	2.561	0.548	4.938	3.326	0.799
A0III	0.013	0.040	−0.003	1.188	0.968	0.147	2.447	1.821	0.333	3.774	2.618	0.552	5.151	3.377	0.805
A3III	0.173	0.136	−0.008	1.348	1.054	0.145	2.605	1.899	0.334	3.930	2.689	0.556	5.304	3.445	0.812
A5III	0.185	0.172	0.031	1.370	1.088	0.186	2.638	1.932	0.377	3.972	2.722	0.603	5.353	3.480	0.861
A7III	0.230	0.234	0.025	1.418	1.150	0.183	2.688	1.994	0.376	4.024	2.784	0.602	5.408	3.541	0.862
F0III	0.241	0.276	0.038	1.435	1.186	0.198	2.711	2.026	0.393	4.051	2.815	0.622	5.439	3.571	0.883
F2III	0.198	0.437	0.060	1.417	1.337	0.226	2.717	2.169	0.427	4.079	2.952	0.662	5.486	3.704	0.929
F5III	0.233	0.451	0.074	1.456	1.352	0.242	2.758	2.186	0.444	4.122	2.971	0.680	5.530	3.726	0.948
G0III	0.555	0.663	0.106	1.812	1.544	0.281	3.144	2.364	0.490	4.533	3.140	0.732	5.961	3.888	1.006
G5III	0.969	0.822	0.127	2.256	1.686	0.307	3.612	2.493	0.522	5.019	3.261	0.770	6.462	4.007	1.048
G8III	1.134	0.883	0.133	2.419	1.740	0.314	3.772	2.543	0.529	5.176	3.307	0.777	6.616	4.049	1.055
K0III	1.313	0.891	0.162	2.597	1.753	0.346	3.948	2.559	0.564	5.351	3.328	0.815	6.789	4.074	1.096
K1III	1.462	0.972	0.162	2.754	1.826	0.346	4.111	2.628	0.565	5.517	3.393	0.816	6.958	4.137	1.098
K2III	1.600	1.047	0.186	2.885	1.897	0.374	4.235	2.696	0.597	5.635	3.458	0.852	7.071	4.200	1.137
K3III	1.852	1.118	0.191	3.148	1.960	0.380	4.507	2.753	0.603	5.915	3.513	0.859	7.356	4.252	1.145
K4III	2.272	1.303	0.198	3.601	2.123	0.391	4.989	2.900	0.619	6.419	3.647	0.878	7.878	4.377	1.168
K5III	2.388	1.345	0.252	3.700	2.175	0.452	5.072	2.959	0.684	6.489	3.712	0.949	7.936	4.448	1.244
M0III	2.651	1.444	0.327	3.969	2.266	0.532	5.345	3.044	0.770	6.763	3.793	1.041	8.211	4.527	1.341
M1III	2.585	1.449	0.313	3.893	2.272	0.518	5.263	3.050	0.757	6.678	3.800	1.028	8.125	4.533	1.328
M2III	2.710	1.513	0.385	4.030	2.337	0.597	5.408	3.117	0.844	6.828	3.870	1.122	8.276	4.607	1.429
M3III	2.608	1.477	0.470	3.923	2.302	0.688	5.298	3.084	0.939	6.716	3.838	1.221	8.163	4.578	1.532
M4III	2.557	1.507	0.629	3.869	2.335	0.858	5.242	3.120	1.121	6.656	3.880	1.415	8.099	4.625	1.736
M5III	1.975	1.547	0.757	3.272	2.390	0.997	4.636	3.186	1.270	6.047	3.954	1.573	7.488	4.707	1.903

Table A3. UVEX/IPHAS colour indices $(U-g)$, $(g-r)$, (He I $-r$) for Pickles supergiants including reddening.

Spectral	$E(B-V)=0.0$			$E(B-V)=1.0$			$E(B-V)=2.0$			$E(B-V)=3.0$			$E(B-V)=4.0$		
type	$U-g$	$g-r$	He I $-r$	$U-g$	$g-r$	He I $-r$	$U-g$	$g-r$	He I $-r$	$U-g$	$g-r$	He I $-r$	$U-g$	$g-r$	He I $-r$
B0I	−1.250	−0.193	0.040	−0.034	0.748	0.186	1.267	1.613	0.368	2.635	2.420	0.585	4.053	3.189	0.834
B1I	−1.159	−0.118	0.034	0.056	0.825	0.186	1.354	1.692	0.374	2.720	2.502	0.596	4.134	3.274	0.851
B3I	−0.951	−0.064	0.041	0.251	0.878	0.190	1.539	1.741	0.374	2.896	2.545	0.593	4.303	3.309	0.845
B5I	−0.852	−0.019	0.052	0.358	0.913	0.206	1.651	1.771	0.395	3.010	2.573	0.619	4.417	3.339	0.875
B8I	−0.659	0.005	0.067	0.543	0.931	0.221	1.828	1.783	0.410	3.179	2.581	0.634	4.578	3.344	0.890
A0I	−0.264	0.047	0.051	0.902	0.977	0.206	2.153	1.832	0.397	3.474	2.632	0.621	4.845	3.397	0.879
A2I	−0.217	0.143	0.046	0.964	1.064	0.202	2.229	1.912	0.394	3.563	2.706	0.620	4.946	3.465	0.878
F0I	0.373	0.224	0.048	1.526	1.141	0.208	2.764	1.986	0.403	4.071	2.780	0.633	5.429	3.541	0.896
F5I	0.378	0.288	0.069	1.543	1.204	0.234	2.793	2.050	0.433	4.111	2.846	0.666	5.480	3.609	0.931
F8I	0.728	0.558	0.077	1.938	1.438	0.244	3.225	2.255	0.446	4.574	3.029	0.681	5.967	3.776	0.948
G0I	0.802	0.740	0.101	2.052	1.610	0.274	3.377	2.420	0.482	4.757	3.190	0.724	6.178	3.934	0.997
G2I	1.052	0.825	0.090	2.320	1.682	0.265	3.658	2.483	0.475	5.049	3.246	0.718	6.477	3.986	0.993
G5I	1.330	0.945	0.114	2.617	1.785	0.293	3.969	2.575	0.507	5.369	3.331	0.754	6.804	4.067	1.032
G8I	1.773	1.108	0.183	3.062	1.948	0.371	4.416	2.738	0.593	5.818	3.496	0.848	7.254	4.234	1.133
K2I	2.377	1.342	0.191	3.703	2.153	0.384	5.085	2.922	0.611	6.508	3.665	0.870	7.960	4.392	1.159
K3I	2.473	1.442	0.243	3.799	2.255	0.442	5.183	3.025	0.675	6.608	3.769	0.939	8.064	4.498	1.234
K4I	2.503	1.524	0.276	3.851	2.329	0.479	5.252	3.095	0.715	6.692	3.837	0.983	8.158	4.565	1.281
M2I	2.676	1.624	0.483	4.002	2.433	0.703	5.383	3.205	0.956	6.804	3.954	1.240	8.254	4.690	1.553

Table A4. UVEX/IPHAS colour indices $(U-g)$, $(g-r)$, (He I $-r$) $(r-\mathrm{H}\alpha)$ and $(r-i)$ for $\log(g) = 8.0$ Bergeron DA white dwarfs including reddening.

T (K)	$E(B-V)=0.0$					$E(B-V)=1.0$					$E(B-V)=2.0$				
	$U-g$	$g-r$	He I $-r$	$r-\mathrm{H}\alpha$	$r-i$	$U-g$	$g-r$	He I $-r$	$r-\mathrm{H}\alpha$	$r-i$	$U-g$	$g-r$	He I $-r$	$r-\mathrm{H}\alpha$	$r-i$
1500	1.809	0.761	−0.232	−0.275	−2.272	3.113	1.469	−0.132	−0.030	−1.598	4.475	2.129	−0.004	0.186	−0.901
1750	1.592	1.025	−0.095	0.007	−1.613	2.895	1.772	0.036	0.220	−0.944	4.258	2.469	0.196	0.404	−0.254
2000	1.419	1.160	0.029	0.215	−1.036	2.719	1.939	0.185	0.403	−0.375	4.082	2.669	0.372	0.561	0.303
2250	1.271	1.229	0.118	0.325	−0.531	2.570	2.034	0.293	0.495	0.124	3.931	2.788	0.499	0.634	0.792
2500	1.141	1.254	0.174	0.375	−0.093	2.437	2.078	0.361	0.534	0.562	3.798	2.849	0.580	0.660	1.227
2750	1.030	1.249	0.203	0.393	0.258	2.324	2.084	0.396	0.545	0.920	3.684	2.867	0.622	0.664	1.590
3000	0.936	1.225	0.214	0.396	0.501	2.228	2.068	0.409	0.546	1.174	3.586	2.858	0.638	0.662	1.853
3250	0.850	1.191	0.214	0.393	0.638	2.140	2.040	0.410	0.542	1.320	3.497	2.834	0.639	0.658	2.007
3500	0.768	1.151	0.209	0.386	0.694	2.056	2.003	0.404	0.536	1.381	3.412	2.800	0.633	0.653	2.073
3750	0.687	1.106	0.201	0.378	0.700	1.972	1.962	0.395	0.529	1.390	3.326	2.762	0.622	0.647	2.085
4000	0.603	1.057	0.191	0.368	0.682	1.885	1.916	0.383	0.522	1.373	3.238	2.718	0.609	0.641	2.070
4250	0.512	1.002	0.180	0.357	0.650	1.791	1.865	0.370	0.513	1.342	3.141	2.670	0.594	0.634	2.039
4500	0.412	0.941	0.168	0.344	0.610	1.688	1.808	0.355	0.502	1.303	3.036	2.615	0.577	0.626	2.001
4750	0.307	0.876	0.155	0.329	0.567	1.580	1.747	0.340	0.490	1.261	2.925	2.558	0.559	0.616	1.959
5000	0.201	0.810	0.143	0.311	0.523	1.470	1.686	0.324	0.474	1.218	2.812	2.499	0.541	0.603	1.917
5250	0.100	0.747	0.130	0.288	0.482	1.365	1.626	0.309	0.453	1.178	2.705	2.443	0.523	0.585	1.877
5500	0.006	0.688	0.118	0.260	0.445	1.268	1.572	0.295	0.428	1.141	2.606	2.391	0.506	0.562	1.842
6000	−0.160	0.584	0.098	0.205	0.381	1.097	1.474	0.270	0.377	1.079	2.430	2.298	0.477	0.516	1.780
6500	−0.303	0.494	0.080	0.157	0.327	0.949	1.390	0.249	0.334	1.026	2.279	2.219	0.452	0.476	1.728
7000	−0.409	0.420	0.066	0.117	0.280	0.839	1.321	0.232	0.297	0.980	2.167	2.152	0.432	0.442	1.684
7500	−0.479	0.360	0.055	0.082	0.240	0.766	1.264	0.217	0.265	0.941	2.092	2.098	0.415	0.412	1.646
8000	−0.520	0.310	0.044	0.048	0.204	0.723	1.216	0.204	0.233	0.906	2.047	2.052	0.400	0.383	1.611
8500	−0.539	0.266	0.034	0.014	0.171	0.702	1.174	0.192	0.202	0.873	2.025	2.010	0.385	0.354	1.579
9000	−0.543	0.228	0.023	−0.022	0.140	0.698	1.136	0.178	0.167	0.843	2.020	1.972	0.369	0.322	1.550
9500	−0.537	0.193	0.011	−0.068	0.110	0.703	1.100	0.164	0.124	0.814	2.025	1.935	0.352	0.282	1.522
10 000	−0.528	0.160	−0.000	−0.119	0.083	0.713	1.067	0.150	0.076	0.788	2.035	1.901	0.335	0.236	1.497
10 500	−0.521	0.132	−0.011	−0.161	0.057	0.719	1.037	0.137	0.037	0.764	2.041	1.869	0.320	0.199	1.474
11 000	−0.522	0.106	−0.019	−0.191	0.035	0.718	1.010	0.127	0.008	0.742	2.040	1.842	0.308	0.173	1.453
11 500	−0.529	0.082	−0.026	−0.212	0.016	0.711	0.987	0.119	−0.011	0.724	2.033	1.818	0.298	0.155	1.435
12 000	−0.536	0.061	−0.031	−0.224	−0.001	0.704	0.966	0.112	−0.021	0.708	2.026	1.797	0.290	0.146	1.420
12 500	−0.543	0.044	−0.034	−0.225	−0.013	0.696	0.949	0.108	−0.022	0.696	2.017	1.781	0.286	0.146	1.408
13 000	−0.554	0.027	−0.036	−0.223	−0.024	0.684	0.933	0.105	−0.020	0.685	2.004	1.766	0.282	0.149	1.398
13 500	−0.572	0.010	−0.038	−0.221	−0.034	0.664	0.918	0.103	−0.017	0.675	1.983	1.752	0.279	0.153	1.387
14 000	−0.597	−0.005	−0.039	−0.217	−0.044	0.639	0.905	0.102	−0.013	0.665	1.957	1.740	0.278	0.157	1.378
14 500	−0.624	−0.019	−0.039	−0.212	−0.051	0.609	0.893	0.102	−0.007	0.657	1.926	1.730	0.277	0.163	1.370
15 000	−0.653	−0.031	−0.039	−0.206	−0.058	0.579	0.882	0.102	−0.001	0.650	1.895	1.721	0.277	0.169	1.363
15 500	−0.683	−0.042	−0.038	−0.199	−0.064	0.548	0.873	0.102	0.006	0.644	1.863	1.713	0.278	0.176	1.356
16 000	−0.712	−0.052	−0.038	−0.192	−0.070	0.518	0.865	0.102	0.013	0.638	1.832	1.706	0.278	0.183	1.350
16 500	−0.741	−0.061	−0.038	−0.184	−0.075	0.488	0.857	0.103	0.020	0.633	1.801	1.700	0.278	0.190	1.345
17 000	−0.769	−0.070	−0.038	−0.177	−0.079	0.460	0.850	0.103	0.027	0.629	1.772	1.695	0.279	0.197	1.340

Table A4 – *continued*

T (K)	$E(B-V)=3.0$					$E(B-V)=4.0$				
	$U-g$	$g-r$	He I $-r$	$r-$ Hα	$r-i$	$U-g$	$g-r$	He I $-r$	$r-$ Hα	$r-i$
1500	5.879	2.761	0.153	0.374	−0.179	7.312	3.380	0.339	0.532	0.566
1750	5.665	3.136	0.385	0.559	0.455	7.101	3.789	0.604	0.685	1.184
2000	5.489	3.368	0.589	0.689	0.998	6.926	4.050	0.834	0.788	1.708
2250	5.338	3.511	0.736	0.742	1.474	6.776	4.216	1.002	0.821	2.169
2500	5.205	3.589	0.830	0.755	1.903	6.642	4.310	1.110	0.821	2.590
2750	5.090	3.617	0.880	0.752	2.269	6.528	4.348	1.166	0.811	2.955
3000	4.992	3.614	0.899	0.747	2.538	6.430	4.350	1.189	0.802	3.229
3250	4.903	3.593	0.901	0.742	2.699	6.341	4.332	1.191	0.797	3.396
3500	4.816	3.562	0.893	0.737	2.770	6.254	4.303	1.184	0.793	3.471
3750	4.730	3.525	0.881	0.733	2.784	6.168	4.267	1.171	0.789	3.488
4000	4.641	3.483	0.867	0.729	2.770	6.078	4.226	1.154	0.786	3.475
4250	4.543	3.436	0.850	0.723	2.741	5.980	4.180	1.136	0.783	3.446
4500	4.436	3.383	0.830	0.717	2.703	5.872	4.128	1.114	0.779	3.409
4750	4.323	3.327	0.810	0.710	2.661	5.759	4.073	1.092	0.773	3.368
5000	4.209	3.271	0.790	0.699	2.620	5.644	4.017	1.069	0.765	3.327
5250	4.100	3.216	0.770	0.684	2.581	5.534	3.964	1.047	0.752	3.289
5500	4.000	3.166	0.751	0.663	2.546	5.433	3.914	1.026	0.733	3.254
6000	3.822	3.076	0.718	0.621	2.486	5.254	3.826	0.989	0.694	3.195
6500	3.669	2.999	0.689	0.584	2.435	5.101	3.750	0.958	0.661	3.145
7000	3.555	2.935	0.666	0.553	2.392	4.986	3.687	0.932	0.633	3.103
7500	3.479	2.882	0.647	0.526	2.354	4.910	3.635	0.911	0.608	3.066
8000	3.433	2.837	0.629	0.499	2.320	4.864	3.589	0.891	0.583	3.032
8500	3.411	2.795	0.612	0.473	2.289	4.841	3.548	0.872	0.559	3.002
9000	3.405	2.756	0.594	0.443	2.260	4.836	3.507	0.851	0.531	2.974
9500	3.411	2.718	0.574	0.405	2.234	4.842	3.468	0.830	0.495	2.948
10 000	3.421	2.682	0.555	0.362	2.209	4.852	3.430	0.809	0.455	2.925
10 500	3.428	2.649	0.538	0.327	2.187	4.859	3.396	0.789	0.422	2.903
11 000	3.427	2.621	0.524	0.302	2.167	4.859	3.366	0.773	0.399	2.884
11 500	3.420	2.596	0.512	0.287	2.150	4.852	3.341	0.760	0.384	2.867
12 000	3.412	2.575	0.503	0.279	2.135	4.845	3.319	0.750	0.378	2.853
12 500	3.403	2.559	0.498	0.280	2.124	4.835	3.303	0.744	0.379	2.842
13 000	3.389	2.544	0.493	0.283	2.114	4.821	3.288	0.739	0.383	2.832
13 500	3.368	2.531	0.490	0.287	2.103	4.800	3.276	0.735	0.388	2.822
14 000	3.340	2.520	0.489	0.292	2.094	4.771	3.266	0.733	0.393	2.813
14 500	3.309	2.511	0.488	0.298	2.086	4.739	3.258	0.733	0.399	2.804
15 000	3.277	2.504	0.488	0.304	2.078	4.706	3.252	0.732	0.405	2.797
15 500	3.244	2.498	0.488	0.311	2.072	4.673	3.246	0.733	0.413	2.790
16 000	3.212	2.492	0.488	0.318	2.066	4.641	3.242	0.733	0.420	2.784
16 500	3.181	2.487	0.489	0.326	2.060	4.609	3.237	0.733	0.427	2.778
17 000	3.151	2.482	0.489	0.333	2.055	4.579	3.233	0.733	0.434	2.773

Table A5. UVEX/IPHAS colour indices $(U-g)$, $(g-r)$, (He I $-r$) $(r-\mathrm{H}\alpha)$ and $(r-i)$ for $\log(g) = 8.0$ Koester DA white dwarfs including reddening.

T (K)	$E(B-V)=0.0$					$E(B-V)=1.0$					$E(B-V)=2.0$				
	$U-g$	$g-r$	He I $-r$	$r-\mathrm{H}\alpha$	$r-i$	$U-g$	$g-r$	He I $-r$	$r-\mathrm{H}\alpha$	$r-i$	$U-g$	$g-r$	He I $-r$	$r-\mathrm{H}\alpha$	$r-i$
6000	−0.141	0.591	0.102	0.257	0.378	1.115	1.482	0.275	0.429	1.074	2.448	2.306	0.483	0.566	1.775
7000	−0.403	0.423	0.072	0.191	0.275	0.844	1.325	0.238	0.369	0.974	2.171	2.158	0.439	0.513	1.677
8000	−0.517	0.312	0.047	0.101	0.200	0.726	1.219	0.208	0.286	0.901	2.049	2.056	0.404	0.435	1.606
9000	−0.541	0.228	0.024	−0.009	0.139	0.700	1.136	0.179	0.180	0.841	2.022	1.973	0.370	0.335	1.548
10 000	−0.524	0.160	0.000	−0.117	0.083	0.717	1.066	0.151	0.078	0.788	2.039	1.900	0.336	0.239	1.497
11 000	−0.521	0.105	−0.018	−0.183	0.035	0.720	1.010	0.129	0.017	0.742	2.043	1.841	0.310	0.181	1.453
12 000	−0.537	0.063	−0.028	−0.207	0.002	0.703	0.968	0.116	−0.005	0.710	2.024	1.799	0.294	0.162	1.422
13 000	−0.561	0.028	−0.033	−0.208	−0.022	0.677	0.935	0.109	−0.005	0.687	1.997	1.768	0.286	0.164	1.400
14 000	−0.602	−0.004	−0.037	−0.205	−0.042	0.634	0.905	0.104	−0.001	0.667	1.952	1.741	0.281	0.168	1.379
15 000	−0.658	−0.030	−0.037	−0.196	−0.057	0.575	0.883	0.104	0.008	0.651	1.892	1.722	0.279	0.178	1.364
16 000	−0.718	−0.051	−0.037	−0.184	−0.069	0.514	0.866	0.104	0.021	0.639	1.828	1.707	0.280	0.191	1.351
17 000	−0.775	−0.069	−0.036	−0.170	−0.078	0.454	0.851	0.104	0.034	0.629	1.767	1.695	0.280	0.204	1.341
18 000	−0.829	−0.084	−0.036	−0.158	−0.087	0.398	0.838	0.105	0.047	0.621	1.710	1.685	0.280	0.217	1.332
19 000	−0.879	−0.098	−0.036	−0.147	−0.094	0.347	0.827	0.105	0.057	0.613	1.658	1.675	0.280	0.227	1.324
20 000	−0.924	−0.110	−0.036	−0.138	−0.101	0.301	0.816	0.105	0.067	0.606	1.610	1.666	0.280	0.237	1.317
22 000	−1.004	−0.132	−0.036	−0.124	−0.114	0.219	0.798	0.104	0.081	0.593	1.527	1.651	0.279	0.251	1.304
24 000	−1.072	−0.151	−0.037	−0.114	−0.125	0.149	0.781	0.103	0.091	0.581	1.456	1.637	0.278	0.262	1.292
26 000	−1.132	−0.170	−0.037	−0.106	−0.136	0.087	0.766	0.103	0.100	0.571	1.392	1.623	0.277	0.270	1.281
28 000	−1.188	−0.185	−0.037	−0.095	−0.145	0.030	0.752	0.102	0.111	0.561	1.333	1.612	0.277	0.282	1.271
30 000	−1.239	−0.198	−0.037	−0.078	−0.152	−0.023	0.742	0.103	0.127	0.553	1.279	1.603	0.277	0.298	1.263
35 000	−1.322	−0.219	−0.035	−0.038	−0.163	−0.108	0.725	0.105	0.167	0.542	1.192	1.590	0.279	0.337	1.252
40 000	−1.362	−0.231	−0.034	−0.017	−0.169	−0.150	0.716	0.106	0.188	0.536	1.149	1.583	0.280	0.359	1.245
45 000	−1.386	−0.239	−0.034	−0.004	−0.172	−0.175	0.709	0.106	0.201	0.532	1.123	1.578	0.281	0.372	1.241
50 000	−1.403	−0.244	−0.034	0.005	−0.175	−0.193	0.704	0.106	0.210	0.529	1.104	1.574	0.281	0.381	1.238
55 000	−1.416	−0.249	−0.034	0.012	−0.177	−0.206	0.700	0.107	0.217	0.527	1.090	1.570	0.281	0.387	1.236
60 000	−1.427	−0.253	−0.033	0.017	−0.179	−0.217	0.697	0.107	0.222	0.525	1.079	1.568	0.281	0.392	1.234
65 000	−1.435	−0.256	−0.033	0.021	−0.181	−0.226	0.694	0.107	0.226	0.523	1.070	1.565	0.282	0.397	1.232
70 000	−1.443	−0.259	−0.033	0.025	−0.183	−0.234	0.692	0.107	0.230	0.522	1.062	1.563	0.282	0.400	1.230
75 000	−1.449	−0.262	−0.033	0.027	−0.184	−0.241	0.690	0.107	0.232	0.520	1.055	1.562	0.281	0.403	1.229
80 000	−1.455	−0.264	−0.033	0.030	−0.185	−0.247	0.688	0.107	0.235	0.519	1.049	1.560	0.281	0.405	1.227

T (K)	$E(B-V)=3.0$					$E(B-V)=4.0$				
	$U-g$	$g-r$	He I $-r$	$r-\mathrm{H}\alpha$	$r-i$	$U-g$	$g-r$	He I $-r$	$r-\mathrm{H}\alpha$	$r-i$
6000	3.840	3.084	0.724	0.671	2.480	5.272	3.834	0.996	0.744	3.189
7000	3.559	2.942	0.674	0.624	2.384	4.990	3.695	0.941	0.703	3.094
8000	3.435	2.841	0.634	0.551	2.314	4.866	3.594	0.896	0.634	3.026
9000	3.407	2.757	0.595	0.456	2.259	4.838	3.508	0.853	0.544	2.972
10 000	3.426	2.681	0.556	0.364	2.210	4.857	3.429	0.809	0.457	2.925
11 000	3.430	2.620	0.526	0.311	2.167	4.862	3.366	0.775	0.407	2.884
12 000	3.411	2.577	0.507	0.294	2.137	4.844	3.322	0.755	0.393	2.855
13 000	3.383	2.547	0.498	0.297	2.115	4.815	3.292	0.744	0.397	2.834
14 000	3.337	2.521	0.492	0.303	2.095	4.768	3.268	0.737	0.404	2.814
15 000	3.274	2.505	0.490	0.313	2.079	4.705	3.253	0.735	0.414	2.798
16 000	3.209	2.493	0.490	0.326	2.067	4.639	3.243	0.735	0.427	2.785
17 000	3.147	2.483	0.490	0.339	2.056	4.576	3.234	0.735	0.441	2.774
18 000	3.089	2.474	0.491	0.352	2.047	4.517	3.227	0.735	0.453	2.765
19 000	3.036	2.466	0.491	0.363	2.039	4.463	3.220	0.735	0.464	2.756
20 000	2.988	2.459	0.490	0.372	2.031	4.415	3.213	0.734	0.474	2.749
22 000	2.903	2.445	0.489	0.386	2.018	4.329	3.202	0.733	0.488	2.735
24 000	2.831	2.433	0.488	0.397	2.006	4.256	3.191	0.731	0.500	2.723
26 000	2.766	2.421	0.487	0.407	1.995	4.192	3.180	0.730	0.509	2.712
28 000	2.707	2.411	0.486	0.418	1.985	4.131	3.171	0.729	0.521	2.702
30 000	2.652	2.404	0.486	0.434	1.977	4.076	3.166	0.729	0.537	2.693
35 000	2.562	2.395	0.489	0.473	1.964	3.985	3.158	0.732	0.576	2.681
40 000	2.518	2.389	0.490	0.495	1.958	3.940	3.154	0.733	0.597	2.674
45 000	2.492	2.384	0.490	0.508	1.953	3.913	3.150	0.733	0.610	2.669
50 000	2.473	2.381	0.491	0.516	1.950	3.894	3.148	0.734	0.619	2.666
55 000	2.458	2.379	0.491	0.523	1.948	3.879	3.145	0.734	0.625	2.663
60 000	2.447	2.376	0.491	0.528	1.946	3.867	3.144	0.734	0.631	2.661
65 000	2.437	2.375	0.491	0.532	1.944	3.858	3.142	0.734	0.635	2.660
70 000	2.429	2.373	0.491	0.536	1.942	3.849	3.141	0.734	0.638	2.658
75 000	2.422	2.371	0.491	0.539	1.941	3.842	3.139	0.734	0.641	2.656
80 000	2.416	2.370	0.491	0.541	1.940	3.836	3.138	0.734	0.643	2.655

Table A6. UVEX/IPHAS colour indices $(U-g)$, $(g-r)$, (He I $-r$) $(r-\mathrm{H}\alpha)$ and $(r-i)$ for log $(g)=8.0$ Koester DB white dwarfs including reddening.

T (K)	$E(B-V)=0.0$					$E(B-V)=1.0$					$E(B-V)=2.0$				
	$U-g$	$g-r$	He I $-r$	$r-\mathrm{H}\alpha$	$r-i$	$U-g$	$g-r$	He I $-r$	$r-\mathrm{H}\alpha$	$r-i$	$U-g$	$g-r$	He I $-r$	$r-\mathrm{H}\alpha$	$r-i$
10 000	−0.787	0.162	0.033	0.172	0.081	0.444	1.083	0.189	0.361	0.781	1.757	1.930	0.380	0.515	1.485
11 000	−0.874	0.109	0.031	0.161	0.049	0.353	1.033	0.186	0.351	0.749	1.664	1.883	0.375	0.507	1.453
12 000	−0.944	0.067	0.037	0.153	0.023	0.281	0.995	0.190	0.345	0.724	1.590	1.848	0.378	0.502	1.428
13 000	−0.993	0.032	0.050	0.146	−0.000	0.231	0.962	0.202	0.339	0.701	1.539	1.816	0.388	0.498	1.406
14 000	−1.029	0.001	0.072	0.140	−0.020	0.193	0.933	0.223	0.334	0.681	1.500	1.788	0.408	0.494	1.386
15 000	−1.053	−0.024	0.101	0.135	−0.037	0.168	0.908	0.250	0.330	0.665	1.475	1.764	0.435	0.491	1.370
16 000	−1.068	−0.045	0.134	0.130	−0.050	0.153	0.888	0.283	0.326	0.652	1.460	1.744	0.466	0.488	1.358
17 000	−1.077	−0.063	0.167	0.125	−0.060	0.144	0.870	0.314	0.322	0.643	1.451	1.725	0.497	0.485	1.349
18 000	−1.083	−0.078	0.194	0.120	−0.068	0.138	0.855	0.341	0.318	0.635	1.445	1.709	0.522	0.481	1.343
19 000	−1.089	−0.091	0.212	0.115	−0.075	0.132	0.841	0.358	0.314	0.629	1.440	1.695	0.539	0.478	1.337
20 000	−1.095	−0.103	0.220	0.111	−0.081	0.126	0.830	0.366	0.310	0.624	1.433	1.684	0.546	0.475	1.332
22 000	−1.105	−0.117	0.216	0.107	−0.088	0.115	0.816	0.361	0.306	0.617	1.423	1.670	0.541	0.471	1.325
24 000	−1.118	−0.128	0.199	0.104	−0.094	0.102	0.807	0.343	0.304	0.611	1.408	1.662	0.523	0.469	1.319
26 000	−1.141	−0.142	0.185	0.100	−0.103	0.077	0.793	0.329	0.301	0.602	1.383	1.650	0.508	0.467	1.310
28 000	−1.169	−0.156	0.175	0.098	−0.113	0.048	0.781	0.319	0.299	0.592	1.353	1.639	0.497	0.465	1.300
30 000	−1.199	−0.169	0.164	0.096	−0.122	0.018	0.770	0.307	0.297	0.583	1.321	1.630	0.485	0.464	1.291
35 000	−1.270	−0.196	0.134	0.092	−0.139	−0.056	0.747	0.277	0.294	0.565	1.244	1.611	0.454	0.461	1.274
40 000	−1.329	−0.218	0.116	0.088	−0.154	−0.117	0.728	0.258	0.290	0.551	1.182	1.594	0.435	0.459	1.259
50 000	−1.463	−0.236	0.038	0.080	−0.180	−0.256	0.717	0.180	0.284	0.524	1.039	1.589	0.355	0.453	1.232

T (K)	$E(B-V)=3.0$					$E(B-V)=4.0$				
	$U-g$	$g-r$	He I $-r$	$r-\mathrm{H}\alpha$	$r-i$	$U-g$	$g-r$	He I $-r$	$r-\mathrm{H}\alpha$	$r-i$
10 000	3.136	2.722	0.605	0.635	2.193	4.561	3.481	0.863	0.723	2.904
11 000	3.041	2.678	0.598	0.629	2.162	4.466	3.438	0.854	0.719	2.874
12 000	2.967	2.645	0.600	0.626	2.137	4.391	3.406	0.854	0.716	2.849
13 000	2.915	2.614	0.609	0.622	2.114	4.339	3.375	0.863	0.714	2.827
14 000	2.875	2.587	0.627	0.620	2.095	4.299	3.348	0.880	0.713	2.808
15 000	2.850	2.563	0.653	0.618	2.080	4.273	3.324	0.904	0.712	2.793
16 000	2.835	2.542	0.684	0.616	2.068	4.259	3.302	0.934	0.711	2.781
17 000	2.827	2.523	0.713	0.613	2.060	4.252	3.282	0.963	0.709	2.774
18 000	2.822	2.505	0.738	0.610	2.054	4.248	3.264	0.988	0.707	2.768
19 000	2.817	2.491	0.754	0.607	2.048	4.244	3.248	1.003	0.704	2.763
20 000	2.811	2.479	0.761	0.605	2.044	4.237	3.236	1.009	0.702	2.759
22 000	2.800	2.465	0.755	0.602	2.037	4.226	3.222	1.002	0.699	2.752
24 000	2.785	2.458	0.737	0.600	2.031	4.211	3.215	0.984	0.698	2.747
26 000	2.759	2.447	0.722	0.598	2.022	4.185	3.205	0.969	0.696	2.738
28 000	2.728	2.437	0.710	0.597	2.012	4.153	3.196	0.957	0.696	2.728
30 000	2.695	2.429	0.698	0.596	2.003	4.119	3.189	0.944	0.695	2.719
35 000	2.616	2.413	0.666	0.594	1.986	4.039	3.176	0.911	0.694	2.701
40 000	2.552	2.398	0.646	0.592	1.971	3.975	3.162	0.890	0.693	2.686
50 000	2.405	2.399	0.566	0.588	1.943	3.824	3.168	0.810	0.689	2.658

This paper has been typeset from a TEX/LATEX file prepared by the author.